

MAGNETORESISTIVE PROPERTIES OF HOLMIUM AND
CALCIUM DOPED $\text{La}_2\text{BaMn}_2\text{O}_7$ LAYER
COMPOUNDS

M.Phil Thesis

(PHYSICS)

By



Md. Amdadul Hoque
Roll No. 100014004P
Session: October 2000

DEPARTMENT OF PHYSICS

BANGLADESH UNIVERSITY OF ENGINEERING & TECHNOLOGY (BUET)

DHAKA-1000, BANGLADESH





Candidate's Declaration

It is hereby declared that this thesis or any part of it has not been submitted (except publication) elsewhere for the award of any degree or diploma.

Date: 05/09/05
BUET, DHAKA

Md. Amdadul Hoque
(Md. Amdadul Hoque)
Roll No. 100014004P
Session : October 2000


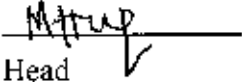
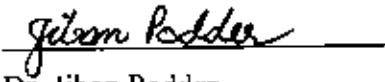
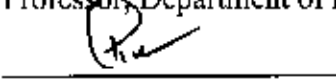
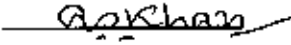
BANGLADESH UNIVERSITY OF ENGINEERING & TECHNOLOGY
Department of Physics, Dhaka-1000, Bangladesh



Certification of Thesis Work

The thesis titled, "Magnetoresistive Properties of Holmium and Calcium Doped $\text{La}_2\text{BaMn}_2\text{O}_7$ Compounds", submitted by Md. Amdadul Hoque, Roll No.: 100014004P, Session: October 2000, has been accepted as satisfactory in partial fulfillment of the requirement for the degree of Master of Philosophy in Physics on 30th August, 2005.

Board of Examiners

1. 
Dr. Mominul Huq
Professor, Department of Physics, BUET, Dhaka
(Supervisor) Chairman
2. 
Head
Department of Physics, BUET, Dhaka Member
3. 
Dr. Jiban Podder
Professor, Department of Physics, BUET, Dhaka Member
4. 
Dr. Md. Feroz Alam Khan
Associate Professor, Department of Physics, BUET, Dhaka Member
5. 
Dr. Abu Sayeed Khan
Professor
Department of Physics
Jahangir Nagar University, Savar Member (external)

ABSTRACT

Magnetoresistive properties of $(La_{2-x}Ho_x)(Ba_{1-y}Ca_y)Mn_2O_7$ bulk polycrystalline samples sintered at temperature 1100°C for 24 hours in air have been investigated from room temperature down to liquid nitrogen temperature using standard four-probe technique. The temperature dependence of normalized resistivity for various polycrystalline samples in zero magnetic field and in a magnetic field of 0.7 Tesla were investigated. The normalized resistivity $\rho(T)/\rho(RT)$ as a function of temperature for various $(La_{2-x}Ho_x)(Ba_{1-y}Ca_y)Mn_2O_7$ polycrystalline samples were measured. X-ray diffraction analysis indicates that the samples are homogeneous and single phase. All double layered manganites show a metal-insulator (M-I) transition at various temperature. This variation of M-I transition in these materials may be due to lattice distortion that occurs mainly for substitution of different cations sizes. The M-I transition temperature is increased only by few Kelvin in presence of 0.7 T applied magnetic field. All samples show magnetoresistance that varies depending on composition. The transport properties above the transition temperature suggest that conduction mechanism in these manganites is a thermally activated process.

Acknowledgements

I express sincere gratitude and thankfulness to my supervisor Professor Dr. Monimul Huq, Department of Physics, Bangladesh University of Engineering & Technology (BUET), Dhaka who gave me an opportunity to carry out this research work under his scholastic supervision. My gratefulness to Professor Huq for his continuous interest in my work, for constant support, fruitful discussion and ideas.

I am also thankful to all the faculty members of the Department of Physics, BUET specially Professor Dr. Md. Abu Hasan Bhuiyan, Professor Dr. Nazma Zaman, Dr. Feroz Alam Khan, Dr. Akther Hossain, Dr. Md Mostak Hossain, Dr. Nazrul Islam and Mr. Md. Rafi Uddin for their encouragement and help during this work.

I express my deepest gratitude to Mohammed Abdul Basith, Lecturer, Department of Physics, BUET for his kind suggestion and support to prepare the present manuscript and also to analyze the experimental results of the dissertation.

Sincere thankfulness to my friend Shabuj for his help and computer facilities. I am also thankful to other M.Phil students of BUET for their kind help. Thanks are also due to staff members of the Physics department of BUET for being incredibly supportive. Thanks to Mr Yusuf Khan for being helpful to perform X-ray diffraction studies for sample characterization.

I am indebted to all of my family members, father, mother, brother, sister and wife for their loving support and inspiration throughout my whole life.

CONTENTS

	Pages
Abstracts	i
Acknowledgements	ii
List of Figures	vi-viii
List of Tables	ix
List of Symbols, Abbreviations and Nomenclature	x
Chapter 1: Introduction	1
1.1 Objectives	3
1.2 Summary of the thesis	3
Chapter 2: Literature Review	6
2.1 Introduction	6
2.2 Materials	8
2.2.1 Structure and electronic spectrum	8
2.2.2 Layered compounds	14
2.3 Properties of CMR materials	15
2.3.1 Intrinsic properties	15
2.3.2 The paramagnetic phase	16
2.4 Transport properties	16
2.4.1 High temperature transport in perovskites-evidence for polarons	16
2.4.2 High temperature resistivity, thermopower	16
2.4.3 Low-temperature transport-low-field magnetoresistance	18

2.4.4	Low-temperature resistivity intergrain transport, Noise	18
2.5	Double Exchange Model	21
2.6	Jahn-Teller distortion	22
2.7	Resistivity and phase diagram	23
2.8	Manganite-Based Device	24
Chapter 3	Sample Preparation and Experimental Techniques	32
3.1	Sample preparation	32
3.1.1	Solid state reaction method	32
3.1.2	Solution Method	32
3.1.3	Melt-quenched or Glass Ceramic Method	32
3.1.4	Thin film Method	33
3.2	Preparation of the Present Samples	33
3.3	Calcinations Schedule	34
3.4	Preparation of pellets	34
3.5	Sintering and oxidation of the pellets	34
3.6	Construction of Liquid Nitrogen Cryostat	35
3.7	Construction of Electromagnet	36
3.8	Construction of the Sample Rod	39
3.9	Magnetoresistance Measurement set-up	41
3.10	The van der Pauw Technique	43
3.11	Magnetoresistance	46
Chapter 4	Results and Discussions	47
4.1	X-ray diffraction analysis	47
4.2	DC Electrical Resistivity	49
4.2.1	DC electrical resistivity of $\text{La}_{2-x}\text{Ho}_x\text{BaMn}_2\text{O}_7$	49
4.2.2	DC electrical resistivity of $\text{La}_2\text{Ba}_{1-y}\text{Ca}_y\text{Mn}_2\text{O}_7$	51

4.2.3	DC electrical resistivity of $\text{La}_{1.9}\text{Ho}_{0.1}\text{BaMn}_2\text{O}_7$ &	53
	$\text{La}_{1.9}\text{Ho}_{0.1}\text{Ba}_{0.8}\text{Ca}_{0.2}\text{Mn}_2\text{O}_7$	
4.2.4	DC electrical resistivity of $\text{La}_{1.8}\text{Ho}_{0.2}\text{BaMn}_2\text{O}_7$ &	
	$\text{La}_{1.8}\text{Ho}_{0.2}\text{Ba}_{0.9}\text{Ca}_{0.1}\text{Mn}_2\text{O}_7$	55
4.3	Magnetoresistance	57
	4.3.1 Magnetoresistance of Various polycrystalline samples	57
4.4	Activation energy	60
Chapter 5	Conclusions and Suggestions for Further Work	65
5.1	Conclusion	65
5.2	Suggestions for further work	66

List of Figures

- Figure 2.1:** Perovskite structure of CaTiO_3 --- 8
- Figure 2.2:** Schematic structures of the Ruddelsden-Popper series of layered compounds. Here n is the number of connected layers of vertex-sharing MnO_6 octahedra. For $n=1$ the structure is that of K_2NiF_4 and $n=2$ is the bilayer structure and $n=\infty$ is the distorted perovskite. The room-temperature lattice parameters are $a=b=3.86 \text{ \AA}$ and $c=12.48 \text{ \AA}$ for $n=1$, $a=b=3.87 \text{ \AA}$ and $c=20.14 \text{ \AA}$ for $n=2$, $a=5.45 \text{ \AA}$ for $n=\infty$ [25].-- 9
- Figure 2.3:** Resistivity against Temperature for $\text{La}_{1-x}\text{Sr}_x\text{MnO}_3$ for various x values. The arrows denote the transition as determined by magnetization measurement [26]. --10
- Figure 2.4:** Top frame-magnetization against temperature for $\text{La}_{0.75}\text{Ca}_{0.25}\text{MnO}_3$ for various field values. Middle frame resistivity against temperature. The inset shows the low temperature resistivity compared to $T^{2.5}$ (solid line) and $T^{4.5}$ (dashed line) behaviour. Bottom frame- magnetoresistance against temperature. Open symbols reflect low-field behaviour and solid symbols reflect the high field behaviour [28]. ---11
- Figure 2.5:** Schematic $T=0$ density of states for doped LaMnO_3 . The level diagram to the left shows the approximate positions of the 3d bands in undoped LaMnO_3 from [24]. The energy scale for $\text{La}_{2/3}\text{Sr}_{1/3}\text{MnO}_3$ is extracted from photoemission data [25]. Comparison is made to Ni metal which possesses a much smaller degree of spin polarization [47]. --13
- Figure 2.6:** Top temperature dependence of the inverse magnetization at $H=1\text{T}$. Bottom in-plane and inter plane resistivity at zero field for the bilayer material $\text{La}_{2-2x}\text{Sr}_{1+2x}\text{Mn}_2\text{O}_7$ ($x=0.3$) single crystal [33]. ---15
- Figure 2.7:** The Seebeck coefficient for $\text{La}_{1-x}\text{Ca}_x\text{MnO}_{3-\delta}$ with varying Ca^{2+} concentration. The arrows indicate the magnetic ordering temperature. (Reproduced from [45].) --18
- Figure 2.8:** Panels a, c and e: the magnetic field dependence of the normalized resistance at various temperatures from 5 to 280 K. Panels b, d and f: the magnetic field dependence of the magnetization (normalized to the 5T value) at various temperatures from 5 to 280K (From Hwang et al. [47]) --20

- Figure 2.9:** Electron states of the outermost 3d energy level of the Mn^{3+} and Mn^{4+} ions -- 21
- Figure 2.10:** Typical resistivity versus temperature curves of $La_{0.7}(Ca_{1-y}Sr_y)_{0.3}MnO_3$ single crystals. The anomaly at a temperature of 370 K for the $y = 0.45$ doping is due to a structural transition from a low-temperature orthorhombic to a high-temperature rhombohedral phase. --23
- Figure 2.11:** Phase diagram of $La_{1-x}Sr_xMnO_3$ ---24
- Figure 2.12:** Optical response of a film of LCMO (closed circles) in comparisons with the TCR (open circles). The R-T curve is shown in the inset [67]. --25
- Figure 3.1:** Schematic diagram of the liquid nitrogen cryostat --36
- Figure 3.2:** Schematic diagram of the Electromagnet. ---37
- Figure 3.3:** Calibration of the home made electromagnet--38
- Figure 3.4:** Schematic diagram of Magnet and Cryostat Assembly for Magnetoresistance Measurements --39
- Figure 3.5:** Schematic diagram of the sample holder --40
- Figure 3.6:** Calibration curve of the temperature sensor (Lakeshore carbon Glass resistor) -40
- Figure 3.7:** A Snapshot of the constructed cryostat. ---41
- Figure 3.8:** Experimental set-up for magnetoresistance measurements.--42
- Figure 3.9:** The four electrical contacts on the circumference of the disc shaped sample.--43
- Figure 3.10:** The function $f(Q)$ for determining the resistivity of the sample(From ref 3)--45
- Figure 4.1:** X-ray diffraction patterns of various polycrystalline samples. ---48
- Figure 4.2:** The zero field normalized resistivity as a function of temperature for various $La_{2-x}Ho_xBaMn_2O_7$ (where $x=0,0.1,0.2$) polycrystalline samples sintered at $1100^\circ C$ in air.--50
- Figure 4.3** The normalized resistivity with constant magnetic field 0.7T as a function of temperature for various $La_{2-x}Ho_xBaMn_2O_7$ (where $x=0,0.1,0.2$) polycrystalline samples sintered at $1100^\circ C$ in air --50
- Figure 4.4** The zero field normalized resistivity as a function of temperature for various $La_2Ba_{1-y}Ca_yMn_2O_7$ (where $y=0,0.1,0.2$) polycrystalline samples sintered at $1100^\circ C$ in air. ---52

- Figure 4.5:** The normalized resistivity with constant magnetic field 0.7T as a function of temperature for various $\text{La}_2\text{Ba}_{1-y}\text{Ca}_y\text{Mn}_2\text{O}_7$ (where $y=0,0.1,0.2$) polycrystalline samples sintered at 1100°C in air. --- 53
- Figure 4.6:** The zero field normalized resistivity as a function of temperature for various $\text{La}_{1.9}\text{Ho}_{0.1}\text{BaMn}_2\text{O}_7$ & $\text{La}_{1.9}\text{Ho}_{0.1}\text{Ba}_{0.9}\text{Ca}_{0.2}\text{Mn}_2\text{O}_7$ polycrystalline samples sintered at 1100°C in air. --- 54
- Figure 4.7:** The zero field normalized resistivity as a function of temperature for various $\text{La}_{1.9}\text{Ho}_{0.1}\text{BaMn}_2\text{O}_7$ & $\text{La}_{1.9}\text{Ho}_{0.1}\text{Ba}_{0.9}\text{Ca}_{0.2}\text{Mn}_2\text{O}_7$ polycrystalline samples sintered at 1100°C in air ---55
- Figure 4.8:** The zero field normalized resistivity as a function of temperature for various $\text{La}_{1.8}\text{Ho}_{0.2}\text{BaMn}_2\text{O}_7$ & $\text{La}_{1.8}\text{Ho}_{0.2}\text{Ba}_{0.9}\text{Ca}_{0.1}\text{Mn}_2\text{O}_7$ polycrystalline samples sintered at 1100°C in air ---56
- Figure 4.9:** The normalized resistivity with constant magnetic field 0.7T as a function of temperature for various $\text{La}_{1.8}\text{Ho}_{0.2}\text{BaMn}_2\text{O}_7$ & $\text{La}_{1.8}\text{Ho}_{0.2}\text{Ba}_{0.9}\text{Ca}_{0.1}\text{Mn}_2\text{O}_7$ polycrystalline samples sintered at 1100°C in air --- 56
- Figure 4.10:** Variation of MR with applied magnetic field at room temperature for various polycrystalline samples. --- 58
- Figure 4.11:** Variation of MR with applied magnetic field at 78K for various polycrystalline samples. --- 58
- Figure 4.12:** Schematic illustration of grain-boundary transport in a polycrystalline mixed-valence manganite. Each grain constitutes a single-magnetic domain. The conduction electrons show a high degree of spin polarization inside the grains. When traveling across the grain boundary conduction electrons may be subject to a strong spin-dependent scattering, which can be reduced if a low external magnetic field aligns the magnetizations of the two grains. Spin alignment in the disordered surface layers gives rise to high-field magnetoresistance -- 60
- Figure 4.13:** $\ln[\rho(T)/\rho(\text{RT})]$ is plotted against $1/T(\text{K}^{-1})$ for various polycrystalline samples at 1100°C sintering temperature. --- 61-63

List of Tables

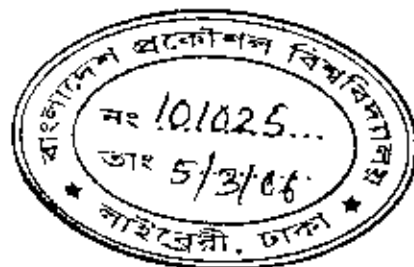
- Table 4.1:** X-ray diffraction peak positions for various polycrystalline samples.--47
- Table 4.2:** The metal-insulator transition temperatures T_p both at zero field and 0.7T applied field for various polycrystalline samples.-- 51
- Table 4.3:** The % MR curve for various polycrystalline samples. ---59
- Table 4.4:** Activation energy of the polycrystalline samples. --61

List of Symbols, Abbreviations and Nomenclature

T_c	-Curie-Weiss transition temperature
T_p	-Phase transition temperature
T_N	-Neel Temperature
K	-Kelvin
°C	-Degree Celsius
K_B	-Boltzmann constant $\cong 1.381 \times 10^{-23} \text{ J/K}$
eV	-Electron volt $\cong 1.609 \times 10^{-19} \text{ J}$
e_g	-Two-fold degenerate state (doublet state)
t_{2g}	-Three-fold degenerate state (triplet state)
DE	-Double exchange
FM	-Ferromagnetic metal
PM	-Paramagnetic metal
CI	-Canted insulator
PI	-Paramagnetic insulator
FI	-Ferromagnetic insulator
MR	-Magnetoresistance
CMR	-Colossal magnetoresistance
GMR	-Giant magnetoresistance
XRD	-X-ray diffraction

Chapter 1

Introduction



This thesis deals with the study of magnetoresistive properties in various divalent and trivalent substituted $\text{La}_2\text{BaMn}_2\text{O}_7$ polycrystalline samples. Recently it was observed that for manganite there is a huge decrease of resistance in presence of magnetic field. This phenomenon is called colossal magnetoresistance (CMR). For manganite magnetoresistance (MR) is very high, it is about 99% for some samples in the presence of applied magnetic field. After the discovery of the colossal magnetoresistance, there has been a renewed interest in the properties of manganites. Generally, the CMR effect is achieved only in presence of a strong magnetic field and with in a small temperature window. These are the two observed constraints of practical applications of CMR materials.

The magnetic and electrical properties of colossal magnetoresistance (CMR) materials were reported in 1950 [1, 2]. The double exchange (DE) model was proposed by zener in the following year [3, 4], to explain the ferromagnetism and metallic behavior observed in these oxide materials of perovskite structure. The perovskite structure is one in a series $(\text{T}_{1-x}\text{D}_x)_{n+1}\text{Mn}_n\text{O}_{3n+1}$ of layer compounds. Here n indexes the number of connected layers of vertex-sharing MnO_6 octahedra. The end points have $n = 1$ and ∞ which corresponds to K_2NiF_4 structure. The $n=1$ compounds particularly $\text{T}_{1-x}\text{D}_x\text{MnO}_3$ materials for $x \approx 0.3$ has been extensively studied because at this composition these materials show a metal-insulator transition at a temperature close to T_c and also shows a colossal magnetoresistive property [5]. For $n = 2$ one has the so-called double layer system. In these compounds, large MR has also been observed for $\text{La}_{2-2x}\text{Sr}_{1+2x}\text{Mn}_2\text{O}_7$ [6] and $\text{La}_{2+2x}\text{Ca}_{1-2x}\text{Mn}_2\text{O}_7$ [7]. Pure $\text{La}_2\text{BaMn}_2\text{O}_7$ is an antiferromagnetic insulator. As a result of adding small amount of divalent cation reducing trivalent & divalent cation (La,Ba) in

$\text{La}_2\text{BaMn}_2\text{O}_7$, the valence state of a few Mn will change from its usual Mn^{3+} to Mn^{4+} . DE model is based on hopping e_g electrons between Mn^{3+} to Mn^{4+} .

Detailed studies [18] have shown that electron-phonon due to Jahn-teller effect is responsible for the observed properties in manganites and a more coherent picture has emerged [8] for the lattice polaron formation associated with the metal-insulator (M-I) transition in these materials. There is also a proposal [9] that M-I transition is a consequence of the large to small polaron transition induced by the reduction of effective hopping integrals at temperature near T_c . Moreover, it has become increasingly evident that the correlation between local structure changes and polaron formation can provide an adequate description for the anomalies observed in many experiment, such as the unusual temperature dependence of Debye-Waller factors and lattice parameters [10], large frequency shifts of the internal infrared modes [11] and variations in the local structure as seen by pair distribution function (PDF) analysis [12]. In spite of above success there are indication that Jahn-Teller polaron formation does not take place in magnetic compound like $\text{La}_{2/3}\text{Sr}_{1/3}\text{MnO}_3$ so that an alternative disorder induced localization mechanism for non-polaronic localization of charge carriers has been introduced. In addition, an empirical spin dependent hopping model [13] has also been suggested to describe the field dependent transport at constant temperatures. Theoretical considerations are still not sufficient and more efficient physical models would have to be developed.

However to explain the decrease of resistance as a result of applied magnetic field in these oxide materials [14-17] led to the conclusion that the DE interaction must be augmented by an interactions between charge carriers and lattice distortions[18]. According to Jonker and Santen [1,2] magnetic properties in these materials can be understood by (1) strong positive (ferromagnetic) interaction between Mn^{3+} and Mn^{4+} (2) weak interaction (either ferromagnetic or antiferromagnetic depending on the distance between them) between Mn^{3+} and Mn^{3+} (3) negative interaction (antiferromagnetic) between Mn^{4+} and Mn^{4+} .

In the present study the parent $\text{La}_2\text{BaMn}_2\text{O}_7$ compound was doped by other divalent and trivalent cations. The small amount of trivalent La was replaced by trivalent Ho and also divalent Ba was replaced by divalent Ca. In this thesis, the polycrystalline $(\text{La}_{2-x}\text{Ho}_x)(\text{Ba}_{1-y}\text{Ca}_y)\text{Mn}_2\text{O}_7$ perovskite was synthesized and magnetoresistive properties as a function of temperature and magnetic field was described.

1.1 Objectives

So far most of the CMR studies have been focused on AMnO_3 -type perovskite oxides that have simple three dimensional structure. In view of the sensitivity of MR properties to the structure, the present study on $(\text{La}_{2-x}\text{Ho}_x)(\text{Ba}_{1-y}\text{Ca}_y)\text{Mn}_2\text{O}_7$ might provide an idea to elucidate fundamental understanding of the CMR mechanism because it has a two-dimensionally layered structure. And as mentioned earlier the structure of the above sample is considered as the $n=2$ member of the Ruddlesden-Popper series $\text{A}_{n+1}\text{B}_n\text{O}_{3n+1}$ in which two perovskite blocks composed by two-dimensional layers of BO_6 corner-sharing octahedral are separated by rock salt AO layers.

1.2 Summary of the thesis:-

The format of the thesis is as follows:

Chapter 2 gives the brief description of the basic issues of CMR in manganites. The phase diagrams of various divalent and trivalent doped manganites. The various models of low temperature, low-field MR are also discussed in this chapter

Chapter 3 gives the details of the sample preparation and experimental techniques used in this thesis.

Chapter 4 describes the results of polycrystalline $(\text{La}_{2-x}\text{Ho}_x)(\text{Ba}_{1-y}\text{Ca}_y)\text{Mn}_2\text{O}_7$ for various x and y values.

Chapter 5 summarizes the finding of this dissertation and makes suggestion for future investigation.

References:

- [1] G.H. Jonker and J.H. Van Santen, "Ferromagnetic compounds of manganese with perovskite structure," *Physica* **16** 337 (1950).
- [2] G.H. Jonker and J.H. Van Santen, "Interaction between the d -Shells in the Transition Metals. II. Ferromagnetic Compounds of Manganese with Perovskite Structure", *Physica* **16** 599 (1950).
- [3] C.Zener, "Interaction between the d -Shells in the Transition Metals. II. Ferromagnetic Compounds of Manganese with Perovskite Structure," *Phys. Rev.* **82** (3), 403-405(1951).
- [4] C.Zener, "Interaction between d shells in the transition metals," *Phys. Rev.* **81**, 440-444, (1951).
- [5] Jun Zhang, H. Tanaka & T. Kawai, "Strain-induced insulator-metal transition and room-temperature colossal magnetoresistance in low-doped $\text{La}_{1-x}\text{Ba}_x\text{MnO}_3$ thin films", *J. Appl. Phys.* **90** 6275 (2001)
- [6] Moritomo Y. Asamitsu A, Kuwahara H and Tskura Y "Photoinduced spin-state transition of Co^{3+} in the layered perovskite manganite thin film", *Nature* **380** 141, (1996).
- [7] Asano H, Hayakawa J and Matsui M., "Giant magnetoresistance of low-dimensional ferromagnet $\text{La}_{2-2x}\text{Ca}_{1+2x}\text{Mn}_2\text{O}_7$.", *Appl. Phys. Lett.* **68** 3638 (1996).
- [8] H. Roder, Jun Zang, and A.R. Bishop, "Lattice Effects in the Colossal-Magnetoresistance Manganites", *Phys.Rev.Lett* **76** 1356 (1996).
- [9] A.J. Millis, Boris I. Shraiman, and R. Mueller, "Dynamic Jahn-Teller Effect and Colossal Magnetoresistance in $\text{La}_{1-x}\text{Sr}_x\text{MnO}_3$ " *Phys.Rev.Lett* **77** 175 (1996)
- [10] Guo-meng Zhou, K. Conder, H. Keller, K.A. Muller, "Strong Oxygen-Mass Dependence of the Thermal-Expansion Coefficient in the Manganites $(\text{La}_{1-x}\text{Ca}_x)_{1-y}\text{Mn}_{1-y}\text{O}_3$ ", *Nature* **381** 676 (1996).
- [11] Chatchai Srinitiwarawong and Michael Ziese, "Polaronic effects on the resistivity of manganite thin films", *App Phys. Lett.* **73**(8), 1140 (1998).

- [12] P.G. Radaelli, D.E.Cox, M. Marezio, S.W. Cheong, P.E.Schiffer, and A.P. Ramirez, "Simultaneous Structural, Magnetic and Electronic Transitions in $\text{La}_{1-x}\text{Ca}_x\text{MnO}_3$ with $x=0.25$ and 0.50 ", *Phys.Rev.Lett* **75** 4488(1995)
- [13] K.H. Kim, J.Y. Gu, H. S. Choi, G.W. Park, and T.W. Noh, "Frequency Shifts of the Internal Phonon Modes in $\text{La}_{0.7}\text{Ca}_{0.3}\text{MnO}_3$ ", *Phys.Rev.Lett.* **77** 1877(1996)
- [14] C.Zener, "Interaction between d shells in the transition metals. ii.Ferromagnetic compounds of manganese with perovskite structure", *Phys. Rev.***82** (3), 403(1951).
- [15] R. von Helmholt et al., "Giant negative magnetoresistance in perovskitelike $\text{La}_{2/3}\text{Ba}_{1/3}\text{MnO}_x$ ferromagnetic films",*Phys.Rev.Lett.* **71** 2331 (1994)
- [16] M.Mc-Cormack et al., "Metal-Insulator Transition and Colossal Magnetoresistance in Manganites",*Appl. Phys. Lett.* **64** 3045 (1994)
- [17] S.Jin et al., "Mössbauer Studies of Fe-doped La-Ca-Mn-O Colossal Magnetoresistive Perovskites",*Science* **264** 413 (1994).
- [18] A.J. Millis et al., "Double Exchange Alone Does Not Explain the Resistivity of $\text{La}_{1-x}\text{Sr}_x\text{MnO}_3$ ",*Phys. Rev. Lett.* **74** 5144 (1995).

Chapter 2

Literature Review

In this chapter the basic issues of the colossal magnetoresistive materials are briefly described. Various phase diagrams that describe the electrical transport and magnetic properties of materials are presented in this chapter. Theoretical explanations of colossal magnetoresistive materials are described. Various models of low temperature and low field MR are also discussed.

2.1 Introduction

The change in electrical resistance in the magnetic material with applied magnetic field is called magnetoresistance (MR). It is very interesting phenomena which helps us to get proper idea in the magnetic field based technology. During the last decade interest has grown in heterogeneous ferromagnetic materials, such as thin film multilayers and cluster-allow compounds which display giant magnetoresistance (GMR). The interest in these systems stem from the prospect of their use in magnetic sensors, magnetoresistive read heads, magnetoresistive random access memory (MRAM). More recently, it was observed that some materials specifically 3d transition metal oxide and carbonates possess a large room temperature magnetoresistivity associated with a paramagnetic to ferromagnetic phase transition. The growth of interest in their properties stem is large part from the prospect of creating metal oxide or carbonate device whose performance exceeds GMR devices. In addition it is now recognized that the large magnetoresistivity in these oxides and carbonate are the result of a unique type of metal semiconductor transition understanding of which complements of the drive for applications

The compounds which have been the focus of the majority of studies are the manganite perovskites $T_{1-x}D_xMnO_3$ where T is a trivalent lanthanide cation (e.g. La, Y etc) and D is divalent (e.g. Ca, Sr, Ba etc), cation. For the end members of the dilution series, $LaMnO_3$ and $CaMnO_3$, the ground state is antiferromagnetic (AF), as expected for spins interacting

via the superexchange interaction where the metal-oxygen-metal bond angle is close to 180° [1]. In a certain range of doping, $x=0.2-0.4$, the ground state is ferromagnetic (FM), and the paramagnetic-to-ferromagnetic transition is accompanied by a sharp drop in resistivity $\rho(T)$. This phenomenon has been known to exist since 1950 [2,3]

Recently, interest in these materials has been renewed by the realization that (i) the magnetoresistance (MR) associated with this correlation between magnetization (M) and resistivity (ρ) can be very large, and (ii) the basic interaction responsible for the ρ -M correlation, the double-exchange (DE) interaction [4-6] between heterovalent (Mn^{3+} , Mn^{4+}) neighbors, is by itself not sufficient to explain this MR[7]. Both the large resistance and the associated MR are now thought to be related to the formation of small lattice polarons in the paramagnetic state. The large MR resulting from the transition has been called colossal magnetoresistance [8], mainly to distinguish it as a phenomenon distinct from GMR. In addition to the renewed interest in the FM state, much attention has been given to another type of collective state, charge order (CO), typically observed for $x>0.3$. At these doping levels CO can compete with the FM ground state, leading to complex electronic phase behaviour as chemical formula is varied [9-11]. Perhaps the biggest intellectual advance in understanding these disparate effects is the realization of the importance of electron-phonon (e-ph) coupling. Several theories have elucidated the role of e-ph coupling in producing CMR [12,13]. It is also widely believed that this e-ph coupling is necessary to explain not only CMR, but also (i) the polaron signatures in transport studies, (ii) the large isotope effect on the FM Curie temperature [14], (iii) the large Debye-Waller factors [15] and (iv) the CO (charge ordering) state and its large sound velocity anomalies [11]. The microscopic origin of strong e-ph coupling is the large Jahn-Teller effect, which occurs for d^4 ions in an octahedral ligand environment [16]. For the undoped material ($x=0$) this results in a large static structural distortions [17]. The question of how this e-ph coupling manifests itself in the CMR range ($x \approx 0.2-0.4$) is one of the central questions to be addressed by theory.

2.2. Materials

2.2.1 Structure and electronic spectrum

Jonker and van santen synthesized and characterized [2] a series of compounds with the general formula $T_{1-x}D_xMnO_3$ where T is a trivalent ion and D is a divalent ion. These compounds form in the structure of perovskite, $CaTiO_3$. In this structure, the T,D and M ions form interpenetrating simple cubic sublattices with O at the cube faces and edges, as shown schematically to the right in figure 2.2. The crystal structure and lattice parameters obtained by neutron powder diffraction are given by Elemans et al for a series of solid solution $La_{1-x}Ba_xMn_{1-y}Ti_yO_3$ [17]. All the compounds studied, which include the end member $LaMnO_3$ are isostructural, crystallizing in the orthorhombic $Pnma$ structure at room temperature. The end member $LaMnO_3$ is very distorted; the octahedral are elongated and tilted. Though tilting distortions are not unusual for perovskites simply on the basis of steric conditions, its magnitude in $LaMnO_3$ and the presence of elongation are thought to be the result of a Jahn-Teller local distortion [17-20]. Jirak et al has shown that for $Pr_{1-x}Ca_xMnO_3$, here exists a phase transition between a high-temperature pseudocubic phase and an orthorhombic phase [21]. This structure at around $x=0.3$, the doping level where the FM state appears, suggesting a strong magneto-elastic coupling. The structure of compounds exhibiting CMR is usually orthorhombic but, as described below in section 2.2, for doping levels near the $T=0$ metal-insulator boundary, the symmetry can be modified by the application of magnetic field.

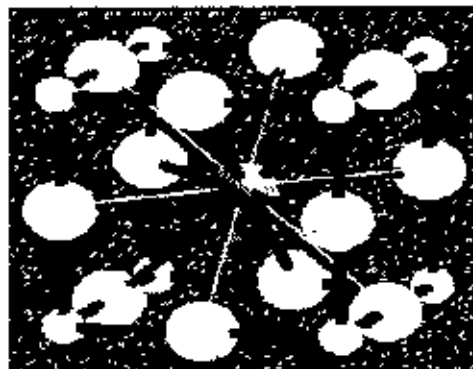


Figure 2.1: Perovskite structure of $CaTiO_3$

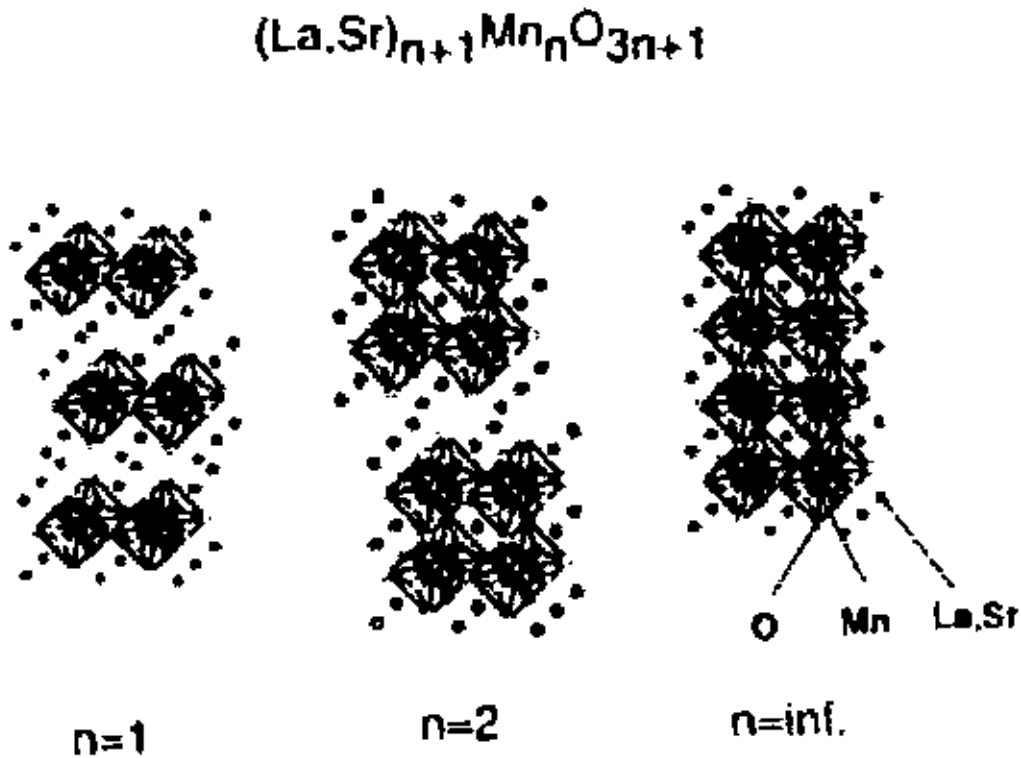


Figure 2.2: Schematic structures of the Ruddlesden-Popper series of layered compounds. Here n is the number of connected layers of vertex-sharing MnO_6 octahedra. For $n=1$ the structure is that of K_2NiF_4 and $n=2$ is the bilayer structure and $n=\infty$ is the distorted perovskite. The room-temperature lattice parameters are $a=b=3.86 \text{ \AA}$ and $c=12.48 \text{ \AA}$ for $n=1$, $a=b=3.87 \text{ \AA}$ and $c=20.14 \text{ \AA}$ for $n=2$, $a=5.45 \text{ \AA}$ for $n=\infty$ [25].

The early work of Jonker and van Santen established the range of possible solid solutions allowed by the Goldschmidt tolerance factor

$$t = (r_D + R_A) / \sqrt{2}(r_T + r_O) \approx 1$$

where r_D , r_T and r_O are the radii of the divalent, trivalent, and oxygen ions, respectively [2]. The tolerance factor measures the deviation from perfect cubic structure ($t=1$). By using mixtures of $T=\text{La, Pr and Nd}$ and $D=\text{Ca, Sr, Ba and Pb}$, t can be varied, with the result that the perovskite structure is stable for $0.85 < t < 0.91$. At finite doping, charge balance is maintained by a fraction, x , of Mn ions assuming a tetravalent, $\text{Mn}^{4+} (d^3)$, configuration in a random fashion throughout the crystal, with the remainder in the $\text{Mn}^{3+} (d^4)$ state.

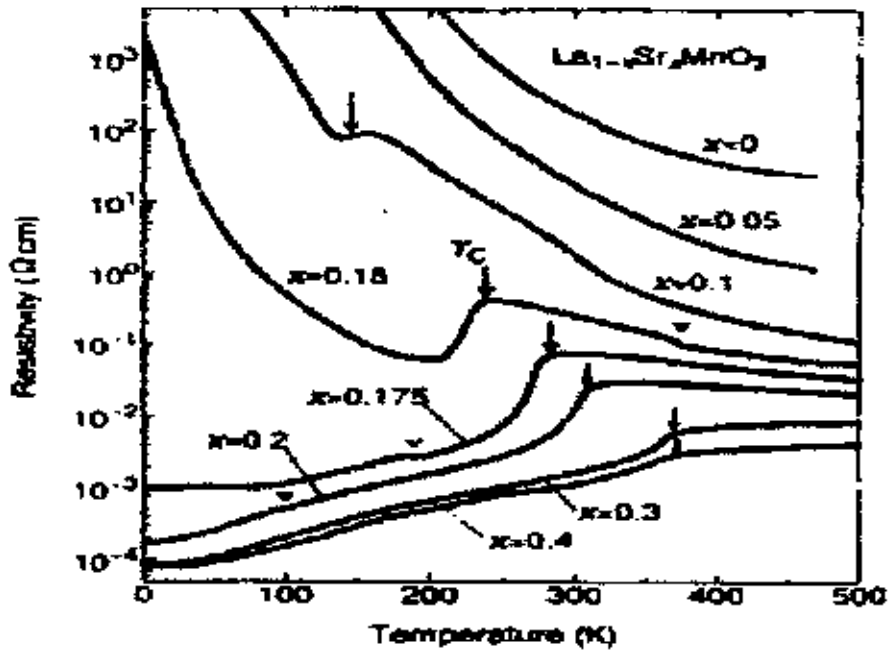


Figure 2.3: Resistivity against Temperature for $\text{La}_{1-x}\text{Sr}_x\text{MnO}_3$ for various x values. The arrows denote the transition as determined by magnetization measurement [26]

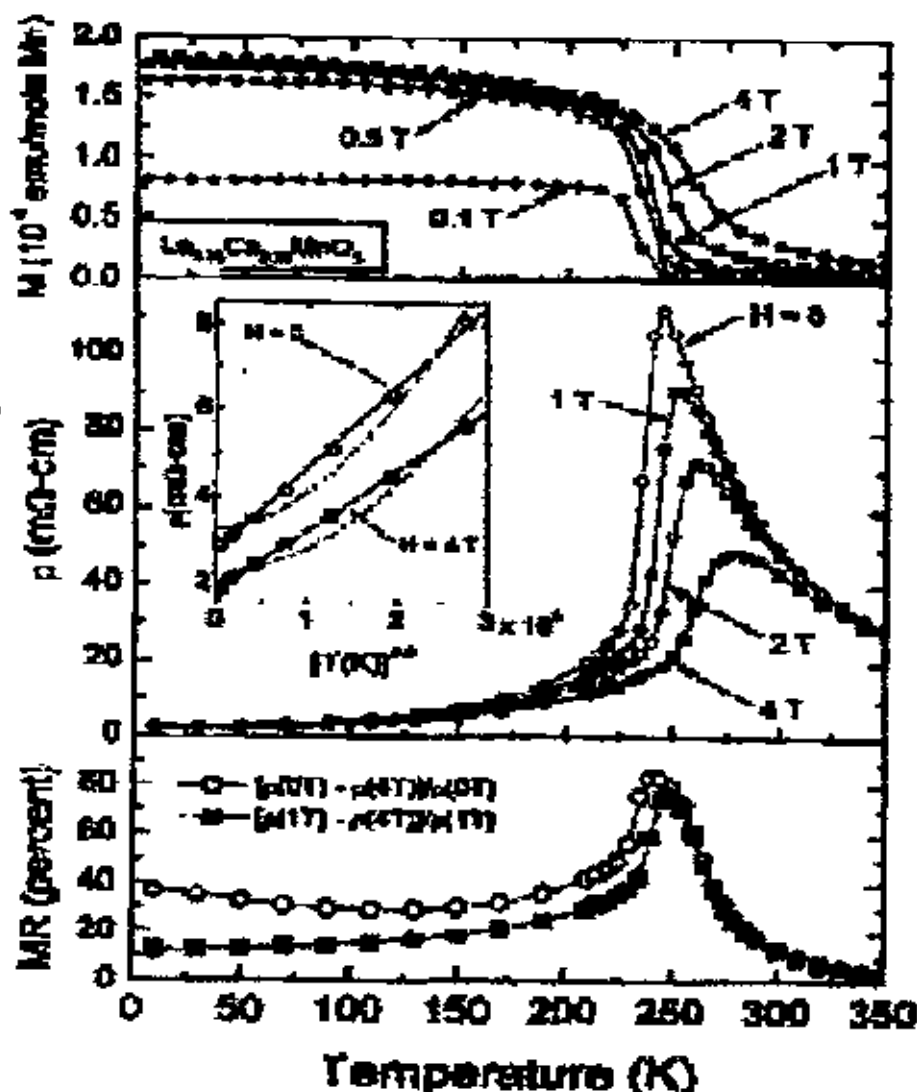


Figure 2.4: Top frame-magnetization against temperature for $\text{La}_{0.75}\text{Ca}_{0.25}\text{MnO}_3$ for various field values. Middle frame resistivity against temperature. The inset shows the low temperature resistivity compared to $T^{2.5}$ (solid line) and $T^{-1.5}$ (dashed line) behaviour. Bottom frame-magnetoresistance against temperature. Open symbols reflect low-field behaviour and solid symbols reflect the high field behaviour [28].

At intermediate values of x , M rises and peaks with its Hund's-rule value at $x=0.3$. In subsequent work [3] van Santen and Jonker showed that at temperatures above the ferromagnetic Curie point, T_0 , the resistivity behaves like a semiconductor, $dp/dT < 0$, but that below T_0 , not only is there a sharp reduction in resistivity, but also a transition to metallic behaviour, $dp/dT > 0$. This behaviour is shown for $\text{La}_{1-x}\text{Sr}_x\text{MnO}_3$ and $\text{La}_{1-x}\text{Ca}_x\text{MnO}_3$ in figures 2.3 and 2.4.

Zener proposed a mechanism, he called double exchange (DE) to explain the simultaneous occurrence of ferromagnetism and metallicity, both as a function of x and T found by Jonker and van Santen [4]. The FM state is observed only for finite d concentration where electronic transport is via holes arising from charge exchange between Ca^{2+} for example, and Mn. For $x < 0.5$ the majority of Mn ions are in the d^4 configuration which, for octahedral coordination, means a half-filled t_{2g} triplet and a quarter-filled e_g doublet. The minorities of sites are d^3 , which corresponds to a half filled t_{2g} orbital triplet. Hund's rule dictates that as the hole hops from site to site, it is accompanied by a reduction in S from 2 to 3/2 (Hund's energy $J_h \gg t$, the transfer integral). This hopping is impeded if neighboring sites are orthogonal, i.e. spins not parallel. Anderson and Hasegawa showed that the transfer integral varies as the cosine of the angle between neighboring spins [5]. As temperature is lowered and spin fluctuations decrease, the combined itinerant local-moment system lowers its total energy by aligning the spins ferromagnetically and allowed the itinerant electrons to gain kinetic energy. Recently, Millis et al have shown that a Hamiltonian incorporating only the DE interaction cannot explain the most obvious feature of the manganites, namely the magnitude of the change in resistivity at the FM transition [8]. They, as well as Roder et al. proposed, in addition to DE, and electron-phonon coupling term [12,13]. Such an interaction is not unexpected in a picture where transition is via hopping among Mn^{3+} and Mn^{4+} ions. Here, the hole, corresponding to a Mn^{4+} (d^3) ion must displace a Mn^{3+} (d^4) ion, which, in the dilute limit, can be associated with a large Jahn-Teller (J-T) coupling. An analysis of acoustic resonance experiments for dilute Cr^{2+} in MgO shows the O^{2-} ions are displaced by roughly 1.5 Å from their undistorted position [16]. Here, Cr^{2+} is, like Mn^{3+} in LaMnO_3 , a d^4 ion in an octahedral oxygen environment. This distortion is of similar magnitude as that in LaMnO_3 and, most likely arises from that manifestation of the strong electron-phonon coupling implied by the J-T theorem in the dilute case. Even though the J-T theorem applies strictly only for single ions, the large distortion found in the acoustic resonance experiments suggests an e-ph coupling of a size which must also play a significant role for interacting ions. Using a different approach, Varma has

attributed the main CMR effect to reduction of localization by spin \uparrow fluctuation scattering with the application of a magnetic field [22].

The picture just outlined, of electronic hopping within narrow and fully spin-polarized bands is supported by a band structure calculation made for the end members of one dilution series, LaMnO_3 and CaMnO_3 [23]. For LaMnO_3 this calculation shows a typical separation between up and down polarized bands of about 1.5 eV and bandwidths of order 1-1.5 eV. Photoemission experiments on $\text{La}_{1-x}\text{D}_x\text{MnO}_3$ (D= Ca,Pb) confirm these basic features [24]. The density of states for such a system is shown schematically in figure 2.5. is also shown for comparison. The density states for Ni metal. Since the up and down spin bands are well separated, the magnetic polarization (saturation moment) is 100%, compared to 11% in Ni. This will lead to reversal of carrier spin direction across FM domains.

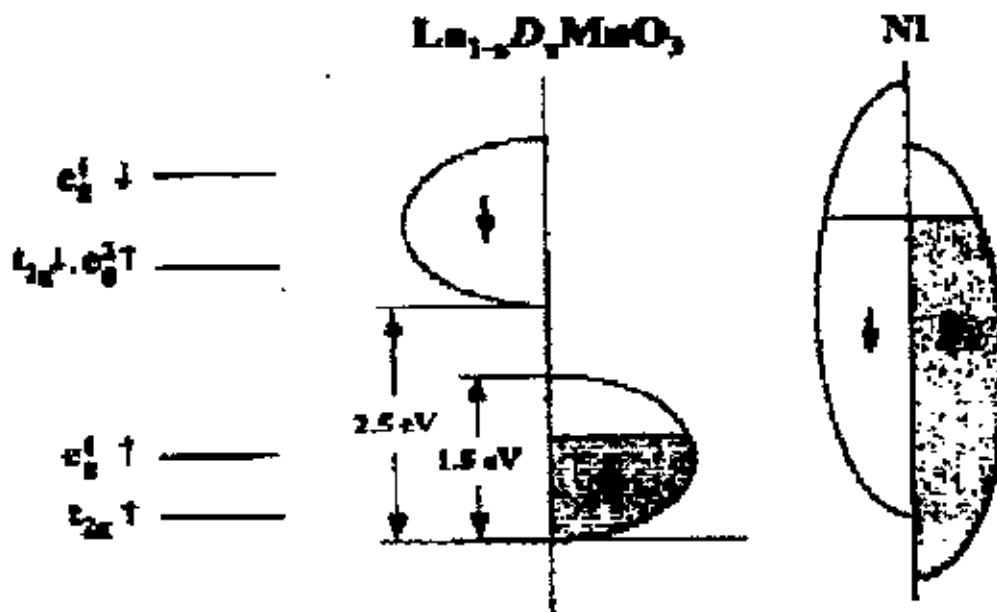


Figure 2.5. Schematic $T=0$ density of states for doped LaMnO_3 . The level diagram to the left shows the approximate positions of the 3d bands in undoped LaMnO_3 from [23]. The energy scale for $\text{La}_{2/3}\text{Sr}_{1/3}\text{MnO}_3$ is extracted from photoemission data [24]. Comparison is made to Ni metal which possesses a much smaller degree of spin polarization [47].

2.2.2 Layered compounds

The perovskite structure is one in a Ruddlesden-Popper series $(T_{1-x}D_x)_{n+1}Mn_nO_{3n+1}$ of layered compounds. Here, n indexes the number of connected layers of vertex sharing MnO_6 octahedra. The endpoints in this series have $n=1$ and ∞ which correspond to the single-layered K_2NiF_4 structure $La_{1-x}Sr_{1+x}MnO_4$ has been well studied [29,30]. These compounds exhibits insulating behaviour for all x , and in the region $x \approx 0.5$, a CO state below about $T \approx 250$ K [29-31]. At lower temperature ($T \approx 20$ K), a spin-glass state appears for $0.2 < x < 0.6$. Spin-glass behaviour is common among manganites with low T_c and presumably reflects the competition between the DE FM interaction and AF superexchange of the present compound $LaMnO_3$. The $x < 0.2$ compounds are AF below $T \approx 100$ K. For $n=2$, one has the so-called double-layer system. In these compounds large MR has also been observed for $La_{2-2x}Sr_{1+2x}Mn_2O_7$ and $La_{2-2x}Ca_{1+2x}Mn_2O_7$ [32] (with this notation, x serves the same role as in the perovskites, denoting the nominal hole concentration). For Ca ($x = 0.25$) a ferromagnetic transition (T_v) of 215 K was identified but the MR peak occurs at a much lower temperature ~ 100 K. The discrepancy between these two temperatures was ascribed by the authors to the quasi-2D nature of the Mn-O layers. For Sr substitution, there are two transitions for $x = 0.4$, one at $T \approx 300$ K which can be attributed to 2D short-range order and a FM transition at $T = 126$ K, below which both c -axis and ab -plane resistivity change from semiconducting ($dp/dT < 0$) to metallic ($dp/dT > 0$). The MR for this compound is much larger than for the 3d ($n = \infty$) system which illustrates the general trend of increasing MR with decreasing T_c . At a slightly lower concentration $x = 0.3$, the $n=2$ system exhibits striking anisotropy in its transport properties.

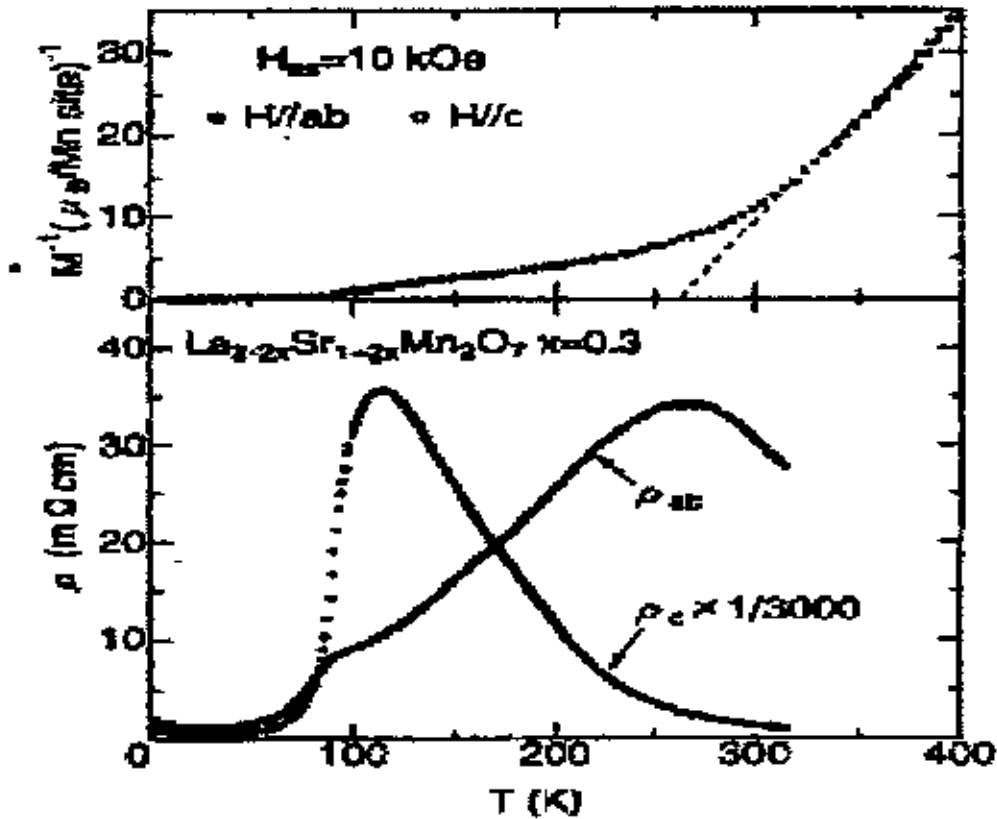


Figure 2.6: Top temperature dependence of the inverse magnetization $H=IT$. Bottom in-plane and interplane resistivity at zero field for the bilayer material $\text{La}_{2-2x}\text{Sr}_{1+2x}\text{Mn}_2\text{O}_7$ ($x=0.3$) single crystal [33].

The effect of different lanthanide-ion substitution has also been studied for the doubly layer system for $\text{LnSr}_2\text{Mn}_2\text{O}_7$ [34,35] where for $\text{Ln}=\text{Tb}$ exhibits a low-temperature magnetization much smaller from that of $\text{Ln}=\text{La}$; for $\text{Ln}=\text{Nd}$, the magnetization is also much smaller than for $\text{Ln}=\text{La}$, and hysteresis reminiscent of spin-glass ordering is seen near 150 k [36,37].

2.3 Properties of CMR Materials

2.3.1 Intrinsic Properties

In magnetism, it is customary to distinguish intrinsic properties, which depends only on the bulk chemical composition and crystal structure, from extrinsic properties which are govern by sample size and microstructure. For example, hysteresis is generally an extrinsic property on the other hand spontaneous magnetization is an intrinsic properties.

2.3.2 The paramagnetic phase

The paramagnetic insulating phase shows thermally activated conduction. The transport mechanism above T_c is still a matter of controversy as different research groups have reported different behaviour. Data on compound with $x \approx 0.3$ were first fitted to

$$\rho = \rho_0 \exp (E_0 / K_B T) \quad (2.1)$$

with an activated energy $E_0 = 0.1-0.2$ eV. Mott's variable range hopping (VRH) expression is given by

$$\rho = \rho_0 \exp (T_0 / T)^v \quad (2.2)$$

with $v = 1/4-1/2$ is appropriate. This also evidence for a

$$\rho \propto \rho_0 \exp (E_0 / KT) \quad (2.3)$$

behaviour over an extended temperature range.

2.4 Transport properties

2.4.1 High temperature transport in perovskites-evidence for polarons

A discussion of the phenomenology of electronic transport in the manganite perovskites can be conveniently separated into three regimes, high-temperature, low-temperature, and critical region. Critical behaviour is best described by thermodynamic measurements, which couple directly to the magnetic correlation length. There is not yet exist a full complement of data to address the critical behaviour . We therefore restrict the discussion to behaviour at low and high temperatures.

2.4.2 High temperature resistivity, thermopower

At high temperature, $T > T_c$, in the concentration region where CMR is strongest, $0.2 < x < 0.4$, transport is characterized by an activated resistivity $\rho(T) \propto \exp(\Delta\rho/T)$ [2] where $\Delta\rho \approx 1000-2000$ K (other reported values are 1100 ± 60 K for $\text{Nd}_{0.5}\text{Pb}_{0.5}\text{MnO}_3$ [26], 1300 K on $\text{La}_{0.76}\text{Ca}_{0.33}\text{MnO}_3$ thin film [38], 2500-1000 K for $\text{La}_{1-x}\text{Ca}_x\text{MnO}_3$ ($0.1 < x < 0.6$) [39], depending on x). The thermopower, $S(T)$, also behaves as expected for a semiconductor, $S(T) \propto \Delta s/T$, where $\Delta s \approx 120$ K [51], 500-20K [39-45] (figure 2.6). In the simplest models, namely that of an intrinsic semiconductor with a single carrier type,

$\Delta\rho=\Delta s$. This experimental work indicates an order-of-magnitude discrepancy between $\Delta\rho$ and Δs , which strongly suggests an additional excitation. It has been suggested, based on the size of the lattice distortion associated with the Jahn-Teller effect for d^4 ions with octahedral coordination, that charge conduction is via small polarons. In the extreme case of noninteracting polarons, there is no entropy transport accompanying charge transport since the polaron energy term in the chemical potential cancels the polaron energy term in the high-temperature expansion of the Kubo formula [59]. In the presence of polaron-polaron interactions however this cancellation does not occur and an extra contribution, of the order of the interaction strength, appears.

Thus in this scenario, $\Delta\rho$ measures the polaron binding energy while Δs measures the polaron-polaron interaction energy. Additional terms will include a spin entropy term, $S_s = (k_B/e) \ln(4/5) \approx 20 \mu\text{V K}^{-1}$ and a configuration (Heikes) entropy term, $S_c = (k_B/e) \ln(1-C_h)/C_h$, where C_h is the fractional hole concentration. It is observed that high temperatures, $S(T)$ extrapolates to a value consistent with S_s , independent of x , presenting a puzzle which is perhaps related to the difference between $\Delta\rho$ and Δs . The thermopower of $\text{La}_{0.67}\text{Ca}_{0.33}\text{MnO}_3$ films in an applied field undergoes the behaviour expected from the known T_c shift and in the critical region displays decreases greater than a factor of 10 for H up to 8T. An alternative, chemistry-based, interpretation of thermopower which seeks to explain the anomalous x -independence at high temperatures is offered by Hundley and Neumeier [45]. The implication that the configurational term, S_c , is nearly x independent is contrary to the expectation that substitution of one Ca ion leads to one mobile hole. They point out that usually $\text{Mn}^{3+}(3d^4)$ is less stable than its neighbours, $\text{Mn}^{2+}(3d^5)$ and $\text{Mn}^{4+}(3d^3)$, and this can lead to disproportionation of Mn^{3+} - Mn^{3+} pairs into Mn^{2+} - Mn^{4+} pairs, a phenomenon not uncommon in transition metal oxides. If one then postulates that only one of the several different Mn valence species is conductive to polaron hopping then as x is varied, not only the number of carriers varied, but also the number of possible sites for transport.

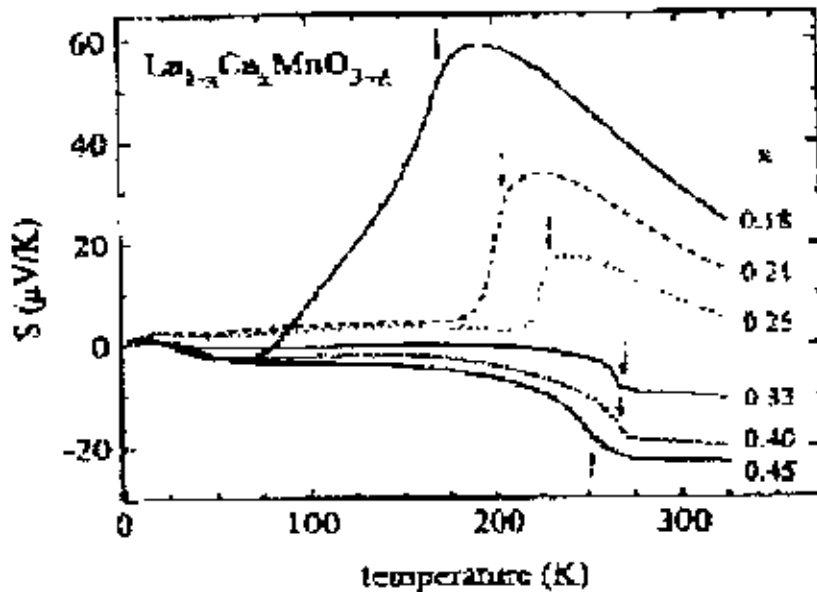


Figure 2.7: The Seebeck coefficient for $\text{La}_{1-x}\text{Ca}_x\text{MnO}_{3-\delta}$ with varying Ca^{2+} concentration. The arrows indicate the magnetic ordering temperature. (Reproduced from [45].)

The configurational contribution, S_c , would therefore depend on the disproportionation probability of Mn^{3+} and after correcting this using existing thermal-gravimetric (TGA) data, good agreement is found with the Heikes formula. This provides an important alternative view of conduction in the manganites, which should be addressed further.

2.4.3 Low-temperature transport-low-field magnetoresistance

The low-temperature transport can be divided into two distinct phenomena, the behaviour of the intrinsic, metallic or semiconducting state, which characterizes high-field MR, and that of the intergrain process which characterizes the low-field behaviour.

2.4.4 Low-temperature resistivity intergrain transport, noise

Ju et al. noticed large low-field magnetoresistance ($\text{MR}_{0.3}=25\%$) in ceramic samples of $\text{La}_{0.67}\text{Ba}_{0.33}\text{MnO}_7$ ($z = 2.99-2.90$) and ascribed this to transport across magnetic domain boundaries. Schiffer et al observed the same effect in ceramic $\text{La}_{0.75}\text{Ca}_{0.25}\text{MnO}_3$, ($\text{MR}_{0.2}=45\%$ at 0.2T) [28]. In this experiment, however, the size of the residual resistivity, $\rho_0=10^{-3}\Omega\text{ cm}$ implied a mean free path of $\sim 10\text{\AA}$, much smaller than a typical

domain size, leading the authors to suggest an additional source scattering in the grain boundaries. Hwang et al demonstrated that this effect was in fact due to scattering by grain boundaries by comparing the low-field MR of polycrystalline $\text{La}_{0.67}\text{Sr}_{0.33}\text{MnO}_3$ and single crystals of the same composition, for which the low field effect is absent [60] (figure 2.8). They showed that the magnitude of the initial drop in $\rho(H)$ varies with temperature which is, characteristic of spin-polarized tunneling in granular ferromagnets [27,48]. Gupta et al. correlated the low-field MR in films of $\text{La}_{0.67}\text{D}_{0.33}\text{MnO}_{3-\delta}$ ($D=\text{Ca, Sr}$ or vacancies) with grain size as measured using transmission electron microscopy (TEM) [49]. They observed no low field MR for epitaxial films and a $\text{MR}_{0.5}\sim 25\%$ at 25K for films with 3 μm grain size. Trilayer devices with junction structure, $\text{La}_{0.67}\text{Sr}_{0.33}\text{MnO}_3/\text{SrTiO}_3/\text{La}_{0.67}\text{Sr}_{0.33}\text{MnO}_3$ show $R_{0.01}\approx 83\%$ at 4.2K[50]. Tunnelling has been directly observed in these devices as a nonlinear I-V characteristic [51].

Mathur et al has fabricated a device that probes the effect of transport across a single grain boundary [52]. They use a bicrystal SrTiO_3 substrate on which is grown a 200nm epitaxial (002) $\text{La}_{0.7}\text{Ca}_{0.3}\text{MnO}_3$ film is grown. A meander line is then patterned from the film across the grain boundary formed at the bicrystal junction. The section of material spanning the grain boundary is one arm of an in situ Wheatstone bridge to further isolate the behaviour of the defect. A peak in the effective resistance of the defect is seen just below T_c and associated with this is an effective $\text{MR}_{0.18}$, which decreases to zero at T_c in a nearly linear fashion. This magnitude of the low-field MR at temperatures close to 300K is larger than that reported by Hwang et al. [47] in polycrystalline material and demonstrates the feasibility of room temperature devices made from CMR material. Finally Hwang et al have achieved large MR at low field using a heterostructure made of $\text{La}_{0.67}\text{Ca}_{0.33}\text{MnO}_3$ sandwiched between two pole pieces of a soft ferromagnet ($\text{Mn, Zn})\text{Fe}_2\text{O}_4$ [53]. Here the applied field is enhanced by the internal field of the pole pieces so the demagnetization field is expected to play an important role in application of this concept to devices.

Central to any discussion of usefulness of CMR materials is whether the MR signal is large compared to the intrinsic noise. Issues of concern are both the high $\rho(T_c)$ values

and the $1/f$ noise related to magnetic domain fluctuations. Alers et al have addressed these issues with noise measurements in $\text{La}_{0.67}\text{Y}_{0.07}\text{Ca}_{0.33}\text{MnO}_3$ thin films [54]. These films had a $\text{MR}_0 > 10^3$ at $T_c = 180\text{K}$. The noise was typically $1/f$ in character and when averaged over the frequency band $\Delta f = 25\text{ Hz}$, had a broad maximum as a function of temperature, peaking below T_c . Due to the $1/f$ character, low-frequency applications near T_c are constrained the equivalent magnetic field noise for a volume of 10^{-12} cm^3 is roughly 10^3 Oe Hz^{-1} . However, at high frequencies, e.g. 10 MHz , the signal to noise ratio for a 1 Oe signal is roughly 20 dB . Thus, while domain-related noise might inhibit incorporation of CMR material for low frequency applications such as magnetic storage, these problems is reduced significantly applications such as reading.

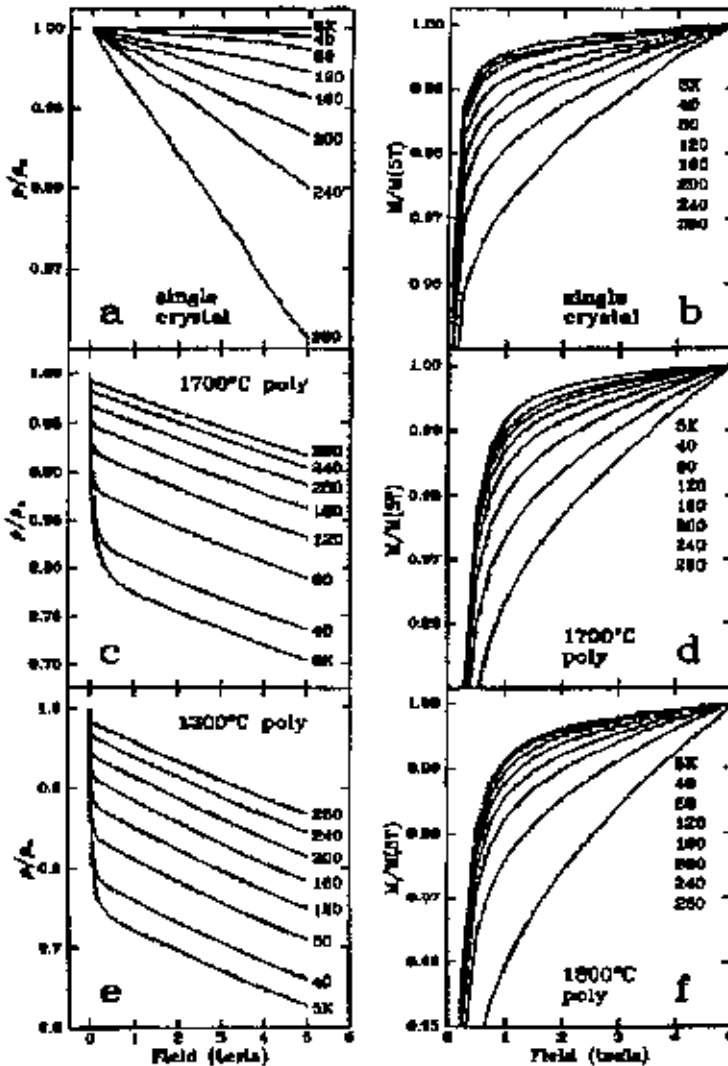


Figure 2.8: Panels a, c and e: The magnetic field dependence of the normalized resistance at various temperatures from 5 to 280 K. Panels b, d and f: The magnetic field dependence of the magnetization (normalized to the 5T value) at various temperatures from 5 to 280K (From Hwang et al. [47])

2.5: Double Exchange Model

The itinerant charge carriers (holes) in the substituted $\text{La}_{1-x}\text{A}_x\text{MnO}_3$ (A is a divalent cation) provide the mechanism of ferromagnetic interaction between Mn^{3+} and Mn^{4+} ions. The addition of divalent material in undoped LaMnO_3 changes the valence state of some Mn^{3+} to Mn^{4+} . The Mn^{3+} ions in LaMnO_3 have three electrons in the t_{2g} state and one electron in the e_g state due to the crystal field splitting. Because of the strong Hund coupling and on-site Coulomb repulsion between e_g electrons, LaMnO_3 is an antiferromagnetic insulator. When trivalent La^{3+} ions are replaced with any divalent cations (e.g., Ca, Sr, Ba etc.), some Mn ions change to the Mn^{4+} state without e_g electrons. The vacant e_g state of Mn^{4+} makes it possible for e_g electrons in surrounding Mn^{3+} ions to hop into the e_g state of Mn^{4+} as long as the localized t_{2g} spins of neighbouring Mn^{3+} and Mn^{4+} ions are parallel.

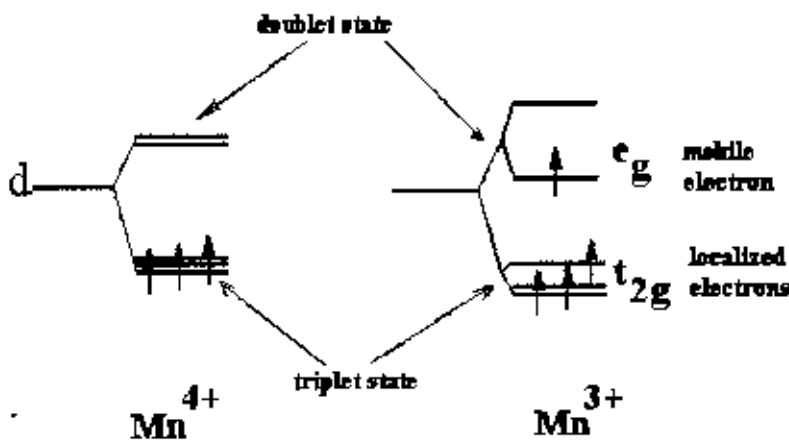
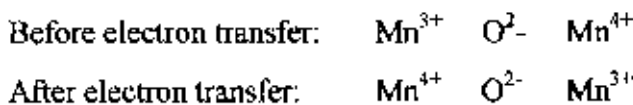


Figure 2.9: Electron states of the outermost 3d energy level of the Mn^{3+} and Mn^{4+} ions

In the perovskite structure the Mn ions are separated by O^{2-} ions and the conduction process occurs via oxygen as follows:



Jonker and van Santen [2], and Wollan and Koehler [55], concluded that the exchange coupling in general is

- (a) ferromagnetic between Mn^{3+} and Mn^{4+} ions
- (b) antiferromagnetic between Mn^{4+} ions.
- (c) either ferromagnetic or antiferromagnetic between Mn^{3+}

The T_c is related to the strength of the transfer integral between Mn^{3+} and Mn^{4+} ions. It can be expected that this coupling is strongly dependent on the angle subtended by the Mn^{3+} -O- Mn^{4+} bond [56]. It is found that the T_c is reduced by bending the Mn^{3+} -O- Mn^{4+} bond [57-60]. Although the ferromagnetism in these materials is attributed to the double exchange mechanism mediated by Mn^{3+} -O- Mn^{4+} , the origin of M-I transition in these materials remains a subject of considerable debate. Millis *et al.* [61-63], have argued that the double exchange mechanism alone is not sufficient to account for a disorder driven M-I transition in this system and conclude that lattice distortion plays a necessary and crucial role in the M-I transitions and the resulting CMR effect. In spite of the intensive research effort, which is currently ongoing, the coupling between crystallographic structure and the electrical and magnetic properties is not completely understood and control of the CMR in this system is still challenging.

2.6: Jahn-Teller distortion

Most researchers agree that double exchange is the basic mechanism underlying the transport properties of the manganites; it seems, however, not to be sufficient to explain the experimental results. Millis *et al.* [64] were among the first to promote the idea that 'double exchange alone does not explain the resistivity of $La_{1-x}Sr_xMnO_3$ ' and concluded that lattice distortion plays a necessary and crucial role in the M-I transitions and the resulting CMR effect. Simply lattice distortion occurs due to their different atomic sizes, crystal structure and different magnetic moments.

A simple inspection is enough to discover sources for distortion. Firstly, ionic size mismatches: cations A and B can have very different sizes producing tilting and twisting of the oxygen octahedra [65, 66]. This distortion can be estimated by the so-called Goldschmidt tolerance factor:

$$\Gamma = \frac{r_{Mn} + r_O}{\sqrt{2}(r_{A/B} + r_O)}$$

where r stands for the sizes of the different ions in the system. $\Gamma=1$ for a cubic lattice and decrease as the difference in size between A and B increases. It has been found that for oxides and fluorides the perovskite structure types are stable in the range

$$1.0 \geq \Gamma \geq 0.77$$

Tilting of the octohedra can be measured with the distortion of the Mn-O-Mn bond angle $\theta=180^\circ$ for cubic symmetry. For particular compositions, θ can range from 150° to 180° .

2.7: Resistivity and phase diagram

CMR manganites are oxides of the type $R_{1-x}A_xMnO_3$, where R denotes a rare earth and A is a divalent, often alkaline earth element.

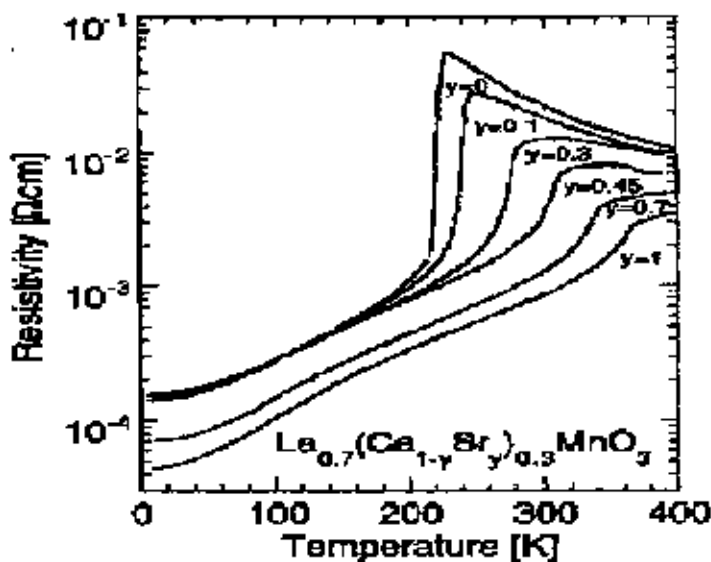


Figure 2.10: Typical resistivity versus temperature curves of $La_{0.7}(Ca_{1-y}Sr_y)_{0.3}MnO_3$ single crystals. The anomaly at a temperature of 370 K for the $y = 0.45$ doping is due to a structural transition from a low-temperature orthorhombic to a high-temperature rhombohedral phase.

Typical resistivity versus temperature curves for $La_{0.7}(Ca_{1-y}Sr_y)_{0.3}MnO_3$ single crystals are shown in figure 2.10. At low temperature the resistivity is metallic, rising sharply while going through the ferromagnetic transition and showing semiconducting behavior in the paramagnetic phase in the case of Ca doping, whereas the resistivity in the case of Sr doping remains metallic above the Curie temperature. Accordingly, the ferromagnetic transition in this compound is accompanied by a metal-insulator transition as evidence by the resistivity rise and the negative temperature coefficient of the resistivity in most compounds above T_c .

Much interest has been devoted to the CMR manganites, since these displays a diversified phase diagram

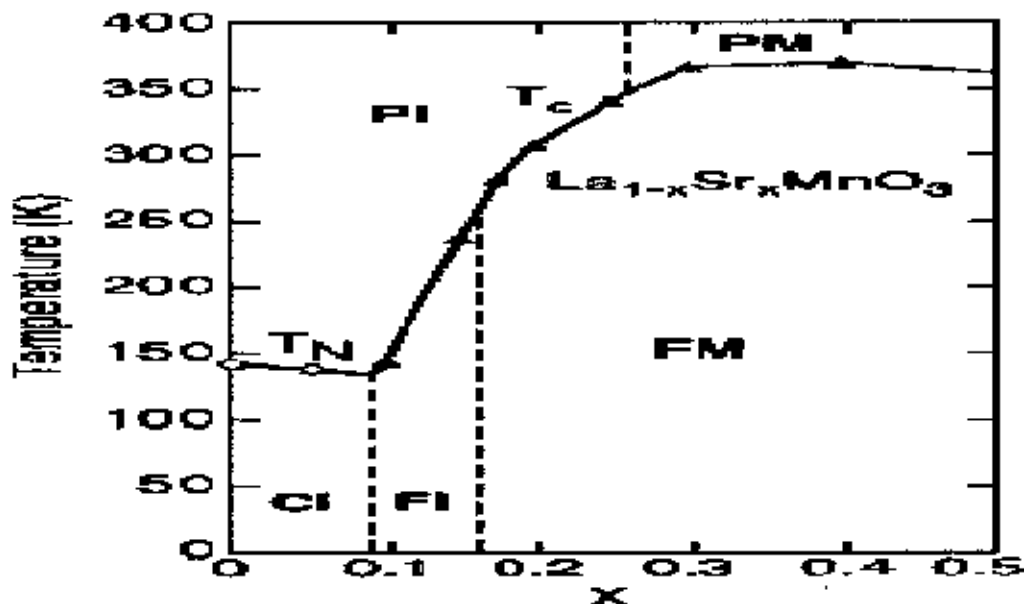


Figure 2.11: Phase diagram of $\text{La}_{1-x}\text{Sr}_x\text{MnO}_3$

2.8 Manganite-Based Device

Based on the properties discussed above, a number of device approaches are being explored, and we will discuss them sequentially as below:

- (i). **Magnetic field sensors** (a) using the CMR effect in a film (b) using a spin valve structure, and (c) as a microwave CMR sensors. The industrial requirements for a magnetic sensor are operation at room temperature and up to 400K, at least a 20% MR at a field 10 mT applied field, temperature independent CMR values over 350 ± 50 K and acceptable noise values. The current thinking is that oxide-based CMR sensors will have maximum impact only on memory systems approaching densities of 100 Gb cm^{-2} .
- (ii). **Electrical field effect devices** (a) using a SrTiO_3 gate and (b) using a ferroelectric gate. Field Effect Transistors (FET) based on CMR channels show some interesting characteristic depending on the dielectric layer on top as to whether it is a pit is a paraelectric layer, such as STO, or a ferroelectric layer, such as PZT. The advantage of these devices unlike conventional NVRAM would be that the reading of the state of memory would be direct since the resistances are considerably different in the two states thus will not require of the memory.

of memory would be direct since the resistances are considerably different in the two states thus will not require of the memory.

(iii). **Room Temperature Bolometric Infrared (IR) sensors**

Due to the advantage in thermoelectric cooling, materials with high thermal nonlinearities in the temperature range of 250-300 K, are potential candidates for bolometric sensors. The commercial bolometers based on VO_x used now a days use temperature coefficient of resistance (TCR) values around 2.5% to 4%. In comparison TCR values ranging from 8% to 18% are possible in the LCMO manganites over the same temperature range (figure 2.12).

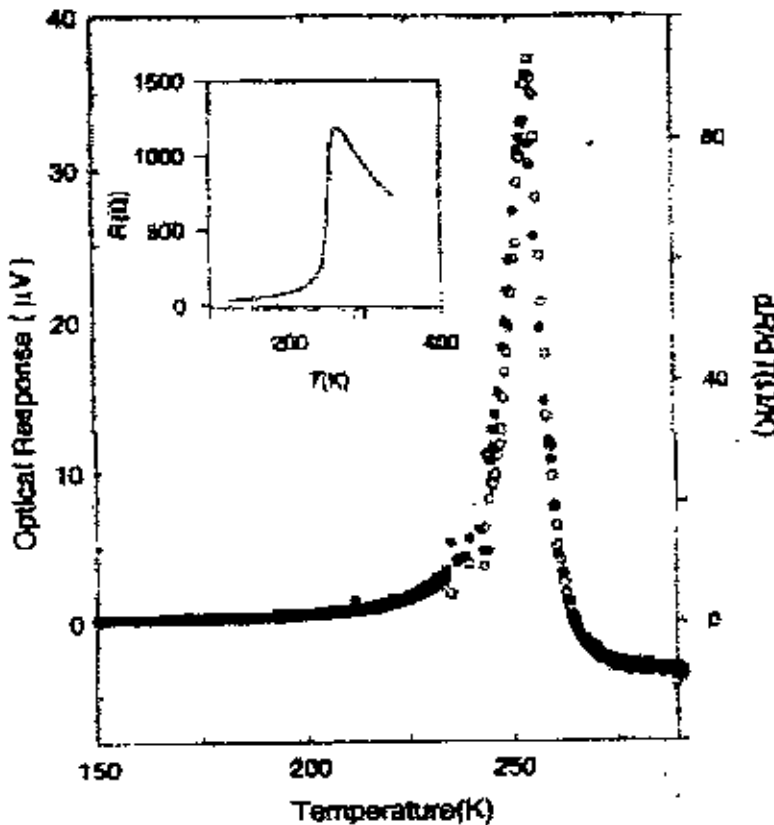


Figure 2.12: Optical response of a film of LCMO (closed circles) in comparisons with the TCR (open circles) The R-T curve is shown in the inset [67]

(iv). **Low temperature hybrid HTS-CMR devices**

As the properties of CMR materials are quite spectacular at reduced temperatures, i.e., below 100K, there may be some advantages to integrating them with HTS devices.

References

- [1] J.B. Goodenough "Magnetism and the Chemical Bond" (Huntington: Krieger) (1976)
- [2] G.H. Jonker and J.H. Van Santen, "Ferromagnetic compounds of manganese with perovskite structure," *Physica* **16** 337 (1950)
- [3] J.H. Van Santen and G.H. Jonker, "Electrical conductivity of ferromagnetic compounds of manganese with perovskite structure," *Physica* **16** 599 (1950)
- [4] G.H. Jonker and J.H. Van Santen, "Magnetic materials containing LaSr manganite phase." *Phys. Rev.* **81** 599 (1951)
- [5] P.W. Anderson and H. Hasegawa, "Considerations on double exchange," *Phys. Rev.* **100** 675 (1955)
- [6] P.G. De genes, "Effects of double exchange in magnetic crystals" *Phys. Rev.* **118** 141 (1960)
- [7] A.J. Millis, P.B. Littlewood and B.I. Shraiman, "Double exchange alone does not explain the resistivity of $\text{La}_{1-x}\text{Sr}_x\text{MnO}_3$," *Phys. Rev. Lett.* **74** 5144 (1995)
- [8] S. Jin, T.H. Tiefel, M. McCormack, R.A. Fastnacht, R. Ramesh and J.H. Chen, "Thousand-fold change in resistivity in magnetoresistive La-Ca-Mn-O films," *Science* **264** 413 (1994)
- [9] Y. Tomioka, A. Asamitsu, Y. Moritomo, H. Kuwahara and Y. Tokura, "Low-field colossal magnetoresistance in bandwidth-controlled manganites", *Phys. Rev. Lett.* **74** 5104 (1995)
- [10] E.O. Wollan and W.C. Koehler, "Neutron diffraction study of the magnetic properties of the series of perovskite-type compounds $[(1-x)\text{La},x\text{Ca}]\text{MnO}_3$," *Phys. Rev.* **100** 545 (1955)
- [11] A.P. Ramirez, P. Schiffer, S.W. Cheong, W. Bao, T.F.M. Palstra, P.L. Gammel, D.J. Bishop and B. Zegarski, "Thermodynamic and Electron Diffraction Signatures of Charge and Spin Ordering in $\text{La}_{1-x}\text{Ca}_x\text{MnO}_3$," *Phys. Rev. Lett.* **76** 3188 (1996)
- [12] A.J. Millis, B.I. Shraiman and R. Mueller, "Dynamic Jahn-Teller effect and colossal magnetoresistance in $\text{La}_{1-x}\text{Sr}_x\text{MnO}_3$," *Phys. Rev. Lett.* **77** 175 (1996)

- [13] H. Rode, J. Zhang and A.R. Bishop, "Lattice effect in the colossal magnetoresistance manganites," *Phys. Rev. Lett* **76** 1356 (1996)
- [14] G. Zhao, K. Conder, H. Keller and K.A. Muller, "Giant oxygen isotope shift in the magnetoresistive perovskite $\text{La}_{1-x}\text{Ca}_x\text{MnO}_{3+y}$," *Nature* **381** 676 (1996)
- [15] P. Dai, J. Zhang, H.A. Mook, S.H. Liou, P.A. Dowben and E.W. Plummer, "Lattice and Static/Dynamic Jahn-Teller Effects in $\text{La}_{1-x}\text{Ca}_x\text{MnO}_3$," *Phys. Rev. B* **54** R3694 (1996)
- [16] J.R. Fletcher and K.W.H. Stephens, "Thermodynamic and Electron Diffraction Signatures of Charge and Spin Ordering in $\text{La}_{1-x}\text{Ca}_x\text{MnO}_3$," *J. Phys. C: Solid State Phys.* **2** 444 (1969)
- [17] J.B.A.A. Elemans, B. VanLaar, K.R. Van Der Veen and B.O. Loopstra, "The crystallographic and magnetic structure of $\text{La}_{1-x}\text{Ba}_x\text{Mn}_{1-x}\text{Me}_x\text{O}_3$," *J. Solid State Chem.* **3** 238 (1971)
- [18] Y. Shimakawa, Y. Kubo and T. Manako, "Giant magnetoresistance in $\text{Tl}_2\text{Mn}_2\text{O}_7$ with the pyrochlore structure," *Nature* **379** 53 (1996)
- [19] A.P. Ramirez, R.J. Cava and J. Krajewski, "Colossal magnetoresistance in Cr based chalcogenide spinels," *Nature* **386** 268 (1997)
- [20] J.B. Goodenough, "Theory of the Role of covalency in the perovskite-type manganites [$\text{La}_x\text{M(II)}\text{MnO}_3$]," *Phys. Rev.* **100** 564 (1955)
- [21] Z. Jirak, S. Krupicka, Z. Simsa, M. Dlouha and S. Vratislav, "Phase separation in structural and magnetic transitions in $\text{Pr}_{0.5}\text{Ca}_{0.5-x}\text{Sr}_x\text{MnO}_3$ ($x=0.15$ and 0.3)", *J. Magn. Magn. Mater.* **53** 153 (1985).
- [22] C.M. Varman, "Electronic and magnetic states in the giant magnetoresistive compounds," *Phys. Rev. B* **54** 7328 (1996).
- [23] S. Satpathy, Z.S. Popovic and F.R. Vukajlovic, "Origin of Charge-Orbital Order in the Half-Doped Manganites", *Phys. Rev. Lett.* **76** 960 (1996).
- [24] J.H. Park, C.T. Chen, S.W. Cheong, W. Bao, G. Meigs, V. Chakarian and Y.U. Idzerda, "Electronic aspects of the ferromagnetic transition in manganese perovskites," *Phys. Rev. Lett.* **76** 4215 (1996).
- [25] Y. Moritomo, A. Asamitsu, H. Kuwahara and Y. Tokura, "Giant Magnetoresistance manganese oxides with a layered perovskite structure," *Nature* **380** 141 (1996).

Chapter 2 Literature Review

- [26] A. Urushibara, Y. Moritomo, T. Arima, A. Asamitsu, G. Kido and Y. Tokura, "Insulator-metal transition and giant magnetoresistance in $\text{La}_{1-x}\text{Sr}_x\text{MnO}_3$ ", *Phys Rev. B* **51** 14 103 (1995).
- [27] J.S. Helman and B. Abeles, "Tunneling of Spin-Polarized Electrons and Magnetoresistance in Granular Ni Films", *Phys. Rev. Lett.* **37** 1429 (1976).
- [28] P. Schiffer, A.P. Ramirez, W. Bao and S.W. Cheong, "Low temperature magnetoresistance and the magnetic phase diagram of $\text{La}_{1-x}\text{Ca}_x\text{MnO}_3$ ", *Phys. Rev. Lett.* **75** 3336 (1995).
- [29] Y. Moritomo, Y. Tomioka, A. Asamitsu, Y. Tokura and Y. Matsui, "Magnetic and electronic properties in hole-doped manganese oxides with layered structures: $\text{La}_{1-x}\text{Sr}_{1+x}\text{MnO}_4$ ", *Phys. Rev. B* **51** 3297 (1995).
- [30] W. Bao, C.H. Chen, S.A. Carter and S.W. Cheong, "Electronic Phase Separation and Charge Ordering in $(\text{Sr},\text{La})_2\text{MnO}_4$: Indication of Triplet Bipolaron", *Solid State Commun.* **98** 55 (1996)
- [31] B.J. Sternlieb, J.P. Hill, U.C. Wildgruber, G.M. Luke, B. Nachumi, Y. Moritomo and Y. Tokura, "Charge and magnetic order in $\text{La}_{0.5}\text{Sr}_{1.5}\text{MnO}_4$ ", *Phys. Rev. Lett.* **76** 2169 (1996)
- [32] H. Asano, J. Hayakawa and M. Matsui, "Giant magnetoresistance of a two dimensional ferromagnet $\text{La}_{2-2x}\text{Ca}_{1+2x}\text{Mn}_2\text{O}_7$ ", *Appl. Phys. Lett.* **68** 3638 (1996)
- [33] T. Kimura, Y. Tomioka, H. Kuwahara, A. Asamitsu, M. Tamura and Y. Tokura, "Interplane tunneling magnetoresistance in a layered manganite crystal," *science* **274** 1698 (1996)
- [34] P.D. Battle, M.A. Green, N.S. Laskey, J.E. Millburn, M.J. Rosseinsky, S.P. Sullivan and J.F. Vente, "Crystal and magnetic structures of the colossal magnetoresistance manganates $\text{Sr}_{2-x}\text{Nd}_{1+x}\text{Mn}_2\text{O}_7$ ($x=0, 0.1$)", *J.Chem. Mater.* **9**,552 (1996)
- [35] R. Seshadri, C. Martin, A. Maignan, M. Hervieu, C. Raveau and C.N. Rao, "Structure and magnetotransport properties of the layered manganites $\text{Re}_{1.2}\text{Sr}_{1.8}\text{Mn}_2\text{O}_7$," *J. Mater. Chem.* **6** 1585 (1996)
- [36] P.D. Battle et al "Colossal magnetoresistance in $\text{Sr}_{2-x}\text{Nd}_{1+x}\text{Mn}_2\text{O}_7$ ($x=0, 0.1$)," *J.Phys.. Condens. Matter* **8** L427 (1996)

- [37] P.D. Battle, M.A. Green, N.S. Laskey, J.E. Milburn, P.G. Radaelli, M.J. Rosseinsky, S.P. Sullivan and J.F. Vente, "Crystal and magnetic structures of the colossal magnetoresistance manganites $Sr_{2-x}Nd_{1+x}Mn_2O_7$ ($x=0.0,0.1$)," *Phys. Rev. B* **54** 15967 (1996)
- [38] M. Jaime, M.B. Salamon, M. Rubinstein, R.E. Treece, J.S. Horwitz and D.B. Crisey, "High temperature thermopower in $La_{2\beta}Ca_{1\beta}MnO_{3+\delta}$ films: Evidence for polaronic transport," *Phys. Rev. B* **54** 11 914 (1996).
- [39] T.T.M. Palstra, A.P. Ramirez, S.W. Cheong, B.R. Zegarski, P. Schiffer and J. Zannan, "Transport mechanisms in doped $LaMnO_3$: Evidence for polaron formation", unpublished, 1996.
- [40] R.C. Miller, R.R. Heikes and R. Mazelsky, "Magnetoresistance in Metallic Crystals of $La_{1-x}Sr_xCoO_3$ ", *J. Appl. Phys.* **32** (Supplement 2202) (1961)
- [41] J. Fontcuberta, A. Seffar, X. Grandos, J.L. Garcia_munoz, X. Obradors and S. Pinol, "Bandwidth narrowing in bulk $La_{2-3x}Al_{1-3x}MnO_3$ magnetoresistive oxides", *Appl Phys Lett*, **68** 2288 (1996).
- [42] A. Asamitsu, Y. Moritomo and Y. Tokura, "Competing instabilities and metastable states in $(Nd,Sm)_{1/2}Sr_{1/2}MnO_3$ ", *Phys. Rev. B* **53** R2952 (1996).
- [43] T. Hashimoto, N. Isizawa, N. Mizutani and M. Kato, *J. Mater. Res.* **23** 1102 (1988)
- [44] M. Jaime, M.B. Salamon, K. Pettit, M. Rubinstein, R.E. Treece, J. S. Horwitz and D.B. Crisey, "Magnetotransport in doped manganate perovskites", *Appl. Phys. Lett.* **68** 1576 (1996).
- [45] M.F. Hundley and J.J. Neumeier, "Thermoelectric power of $La_{1-x}Ca_xMnO_3$: Inadequacy of the nominal $Mn^{3+/4+}$ valence approach", *Phys. Rev. B* **55** 11 511 (1997).
- [46] S.M. Girvin, "Ionic Conductivity Studies in Superionic Conductors with Binary Mobile Ions Using Multi-Component Lattice Gas Model", *J. Solid State Chem.* **25** 65 (1978).
- [47] H.Y. Hwang, S.W. Cheong, N. P. Ong and B. Batlogg, "Spin-Polarized Intergain Tunneling in $La_{2\beta}Sr_{1\beta}MnO_3$ ", *Phys. Rev. Lett.* **77** 2041 (1996)
- [48] A.E. Berkowitz, J.R. Mitchell, M.J. Carey, A.P. Young, S. Zhang, F.E. Spada, F.T. Parker, A. Hutten and G. Thomas, "Giant magnetoresistance in heterogeneous Cu-Co alloys", *Phys. Rev. Lett.* **68** 3745 (1992)

- [49] A. Gupta, G.Q. Gong, G. Xiao, P.R. duncombe, P. Lecoeur, P. Trouilloud, Y.Y. Wang, V.P. Dravid and J.Z. Sun, "Grain-boundary effects on the magnetoresistance properties of perovskite manganite films," *Pys. Rev. B* **54** R15629 (1996)
- [50] J.Z. Sun, W.J. Gallagher, P.R. Duncombe, L. Krusin-Elbaum, R.A. Altmn, A. Gupta, Y. Lu, G.Q. Gong and G. Xiao, "Magnetotransport in doped manganate perovskites", *Pys. Rev. Lett.* **69** 3266 (1996)
- [51] Y. Lu, X.W. Li, G.Q. Gong, G. Xiao, A. Gupta, P. Lecoeur, J.Z. Sun, Y.Y. Wang and V.P. Dravid, "Large magneto-tunneling effects at low magnetic fields in micrometer-scal epitaxial $\text{La}_{0.67}\text{Sr}_{0.33}\text{MnO}_3$ tunnel junctions," *Phys. Rev. B* **54** R8357 (1996)
- [52] N.D. Mathur, G. Burnell, S.P. Isaac, T.J. Jackson, B.S. Teo, J.L. MacManus-Driscoll, L.F. Cohen, J.E. Evetts and M.G. Blamire, "Large low magnetoresistance in $\text{La}_{0.7}\text{Ca}_{0.3}\text{MnO}_3$ induced by artificial grain boundaries," *Nature* **387** 266 (1997)
- [53] H.Y. Hwang, S.W. Cheong and B. Batlogg, "spin-dependent transport and low-field magnetoresistance in doped manganites", *Appl. Phys Lett.* **68** 3494 (1996)
- [54] G.B. Alers, A.P. Ramirez and S. Jin, *Appl. Phys. Lett.* **68** 3644 (1996)
- [55] E.O. Wollan and W.C. Koehler, "Interplay of spin and orbital ordering in the layered colossal magnetoresistance manganite $\text{La}_{2-2x}\text{Sr}_{1+2x}\text{Mn}_2\text{O}_7$ ($0.5 \leq x \leq 1.0$)", *Phys. Rev.* **100** 545 (1955)
- [56] H.Y. Hwang, S.W. Cheong, P.G. Radaelli, M. Marezio & B. Batlogg, "Lattice Effects on the Magnetoresistance in Doped LaMnO_3 ," *Phys. Rev Lett.* **75** (2), 914 (1995)
- [57] J.L. Garcia-Munoz, J. Fontcuberta, M. Suaaidi, & X. Obradors, "Band-Width narrowing in bulk $\text{La}_{2/3}\text{A}_{1/3}\text{MnO}_3$ magnetoresistive oxides," *J. of Phys. Cond. Matt.* **8** L787 (1996)
- [58] P.S.I.P.N. de Silva, F.M. Richards, L.F. Cohen, J.A. Alonso, M.J. Martinez-Lope, M.T. Casais, T. Kodenkandath & J.L. MacManus-Driscoll, "Transmission electron microscopy and x-ray structural investigation of $\text{La}_{0.7}\text{Ca}_{0.3}\text{MnO}_3$ thin films", *J. App. Phys.* **83** (1),394 (1998)

- [59] J.L. Garcia-Munoz, J. Fontcuberta, B. Martinez, A. Seffar, S. Pinol & X. Obradors, "Transport properties of $\text{La}_{1-x}\text{Sr}_x\text{MnO}_3$ ($L=\text{Pr, Nd}$; $1/4 < x < 1/2$)", *Phys. Rev. B* **55** (2), R-668 (1997)
- [60] M. Lide, J. Rodriguez-Martinez and J. Paul Attfield, "Cation disorder and size effects in magnetoresistive manganese oxide perovskites", *Phys. Rev. B* **58** (5), 2426 (1998)
- [61] A J Millis, P. B. Littlewood, & B.I. Shraiman, "Double exchange alone does not explain the resistivity of $\text{La}_{1-x}\text{Sr}_x\text{MnO}_3$," *Phys Rev. Lett.* **74** 5144 (1995)
- [62] A. J. Millis, R. Mueller, and B.I. Shraiman., "Fermi-liquid-to-polaron crossover. II. Double exchange and the physics of colossal magnetoresistance", *Phys. Rev. B* **54** (8) 5405 (1996)
- [63] A. J. Millis, "Variable-range hopping of small polarons in mixed-valence manganites", *Phil. Trans. R. soc. Lond. A* **356** 1473 (1998)
- [64] Millis A. J., Littlewood P. B. and Shraiman B. I., "Double exchange alone does not explain the resistivity of $\text{La}_{1-x}\text{Sr}_x\text{MnO}_3$ ", *Phys. Rev. Lett.* **74** 5144 (1995).
- [65] Fontcuberta J., Martinez B., Sefar A., Pinol S., Garcia-Munoz J.L. and Obradors X., "Colossal Magnetoresistance of Ferromagnetic Manganites. Structural Tuning and Mechanisms," *Phys. Rev. Lett.* **76** 1122 (1996).
- [66] Radaelli P.G, Iannone G., Marezio M., Hwang H.Y, Cheong S.W, Jorgensen J.D and Argyriou D N, "Structural effects on the magnetic and transport properties of perovskite $\text{A}_{1-x}\text{A}'_x\text{MnO}_3$ ($x = 0.25, 0.30$)," *Phys. Rev. B* **56** 8265 (1997)
- [67] T. Venkatesan, M. Rajeswari, Z.W. Dong, S.B. Ogale & R. Ramesh, "Manganite-based devices: opportunities, bottlenecks and challenges", *Phil. Trans R. soc. Lond. A* **356** 1661 (1998)

Chapter 3

Sample Preparation and Experimental Techniques

In this chapter we outline the basic techniques of sample preparation and experimental technique used in this work. We describe construction of a few home made apparatus. These apparatus are used for the magnetoresistance measurements.

3.1 Sample preparation

Samples can be prepared using any of the following four methods.

3.1.1 Solid state reaction method

In solid state reaction method appropriate amounts of two or more chemicals are carefully ground together and mixed thoroughly in a mortar and pestle or ball mills. Ground powders are then calcined in oxygen at a temperature above 1100 °C for several hours then reground and reheat. This process is continued crystalline phase. This calcined material are then ground to fine powders, palletized in a hydraulic press in air or any controlled atmosphere.

3.1.2 Solution Method

In this method appropriate amount of solid chemicals are at first dissolved in nitric acid. This solution is then dried and then followed by calcinations and sintering treatments. Some times water soluble such as nitrates is used for synthesizing superconducting ceramic materials. The nitrates are dissolved in water and then dried and calcined in a way similar to the solid state reaction method.

3.1.3 Melt-quenched or Glass Ceramic Method

In this method appropriate amounts of mixed powder are taken in a oxides, carbonates etc. crucible are calcined for about two hours below the melting point of the materials. After calcinations the powders are melted at a few hundred degrees Celsius above the melting temperature and held there for a couple of hours. The melts are then poured into a cold iron or brass plate and pressed quickly by another plate to 1 to 2 mm thick sheets.

The glasses thus obtained are then annealed at suitable temperature for different periods of time in air or in any controlled atmosphere.

3.1.4 Thin film Method

Thin film of superconducting materials has been very successfully fabricated using the procedure like Evaporation, Sputtering, and Ion Beam sputtering Laser Evaporation etc. Evaporation is conceptually the simplest of all the deposition techniques. In practice, however, some of the most sophisticated apparatus are used to evaporate epitaxial films of materials under very controlled conditions and these systems are more accurately called molecular electron beam epitaxy system (MBE\EBE) The technique involved utilizes a vacuum system to remove most of the contaminating gases from the deposition chamber. Typical pressures that are obtained in simple evaporations are in the 10^{-7} torr range until the MEB\EBE system requires pressures of less than 10^{-10} torr. The elements or compounds to be evaporated are heated in crucibles by either resistive heating elements or by electron beam heating. Typical evaporations have more than one evaporation sources, and it is possible to obtain systems with as many as six independent sources. The high temperature produced in these sources cause the vapor pressure of the evaporation rise to a level at which a significant amount of these materials can be collected on a substrate that is located can collected on a substrate that is located on a direct optical path from the evaporation. The substrate can typically be at a variety of temperatures, ranging from 77 k to approximately 1300k depending on the required microstructure of the final film. The substrate materials are sapphires Al_2O_3 , MgO, silicou etc.

3.2. Preparation of the Present Samples $(La_{2-x}Ho_x)(Ba_{1-y}Ca_y)Mn_2O_7$

Polycrystalline $(La_{2-x}Ho_x)(Ba_{1-y}Ca_y)Mn_2O_7$ with various x & y ($x=0.0, 0.1, 0.2$ & $y=0.0, 0.1, 0.2$) were prepared by conventional solid state reaction technique. Raw materials La_2O_3 (99.995%), $CaCO_3$ (99.9%), $BaCO_3$ (99.9%), Ho_2O_3 (99.9%) and Mn_2CO_3 (99.9%) used as the starting materials. Then we calculated the amount of each ingredients required calculation. We have calculated the amounts of raw materials for a

total 20g. The chemicals were weighted using a FR series Electric Digital Analytical balance (measuring range 0.0001-210gm), weights being shown by LED display.

The chemicals were weighted out separately and then well mixed and ground in a ceramic mortar using a pestle for 4 to 6 hours in acetone. Then grayish powder thus obtained in the mortar was scraped from its wall and was poured into an alumina crucible. Crucible was previously washed with acetone then with distilled water. Crucibles were placed in the furnace for calcinations purpose.

3.3 Calcinations Schedule:

(a) First the powder was heated from room temperature to 1100 °C in air. The temperature controller was set at 1100 °C for 24 hours. After 24 hours the furnace was turned off and was allowed to cool to room temperature (Furnace cooling). When room temperature was attained, the chunk was taken out from the furnace and was ground until it became powder.

(b) The procedure (a) was repeated further for three times.

After 72 hours of total calcination the chunk was ground again until it became fine powder. The product was usually a complete black powder. The resulting black powder is the required powder.

3.4 Preparation of pellets

Calcined powder is a shining black powder. The calcined powders were then pressed into pellets of 14mm diameter and 1-3 mm thick under a pressure of 12000 PSI for about 1 to 2 minutes using a hard pressure machine.

3.5 Sintering and oxidation of the pellets

The pellet formed inside the mould had a shiny black surface. It was again placed a boat and inserted into the furnace for sintering and oxidation. The sample pellets were sintered at 1100°C in a furnace in air atmosphere. This is the maximum operating temperature for this furnace. Now the samples are ready for magnetoresistance measurements.

3.6 Construction of Liquid Nitrogen Cryostat

A liquid nitrogen cryostat is designed for the purpose of low temperature magneto-transport measurements. It is made up of nonmagnetic concentric stainless steel tubes. It consists of two parts (upper part and lower part) and each part consists of three concentric tubes of three different dimensions. The outer diameter of the upper part of the cryostat is 7.6 cm and inner diameter is 3.2 cm. The outer diameter for lower part is 3.8cm and inner diameter is 3.2 cm. It has three chambers as shown in Figure 3.1. Outer chamber is called vacuum chamber the middle one is cryogen chamber (liquid nitrogen) and the innermost chamber is sample space. Thickness of the wall of each chamber is about 0.2 cm. In the top of the second chamber there are two small pipes connected over the stainless steel plate of upper part of the cryostat, one for inlet of liquid nitrogen gas. The lower part (20 cm long and 3.8 cm diameter) of the cryostat is shorter and narrower compared to the upper part (85 cm long and 7.6 cm diameter). It is made in such a way that the lower part of the cryostat can easily move between the pole pieces of the home made electromagnet. A stainless steel plate connects the lower part and upper part. The top of the upper part is sealed by another stainless steel plate. In the innermost chamber (sample space) there is a sample rod which is made up of stainless steel tube and a flat copper bar. The diameter of the sample rod is chosen in such a manner that it can easily move through the sample space. The top of the sample rod and innermost tubes are air tight connected with a union socket. A carbon glass temperature sensor is used for the measurement of temperature of the sample. It was observed that if the cryostat is filled with liquid nitrogen it takes about 150 minutes to warm up to room temperature.

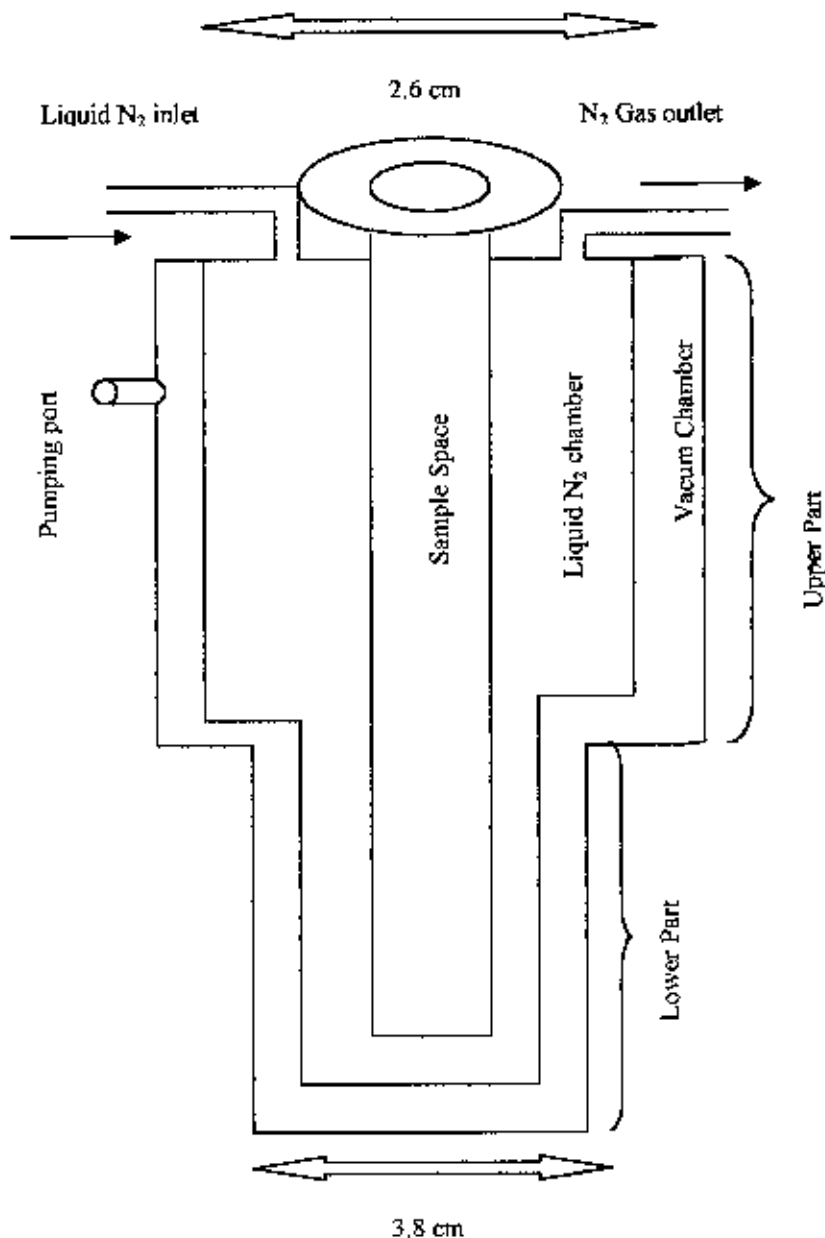


Figure 3.1: schematic diagram of the liquid nitrogen crystal

3.7 Construction of Electromagnet

To study magneto-transport properties of manganese perovskites, an electromagnet was constructed. Normally soft iron with a very low coercive field and low hysteresis is used for the magnet pole pieces. We have used commercial mild steel bar for the body of the electromagnet and soft iron cylindrical rod for pole pieces which are available in the local market (Dhaka, Bangladesh).

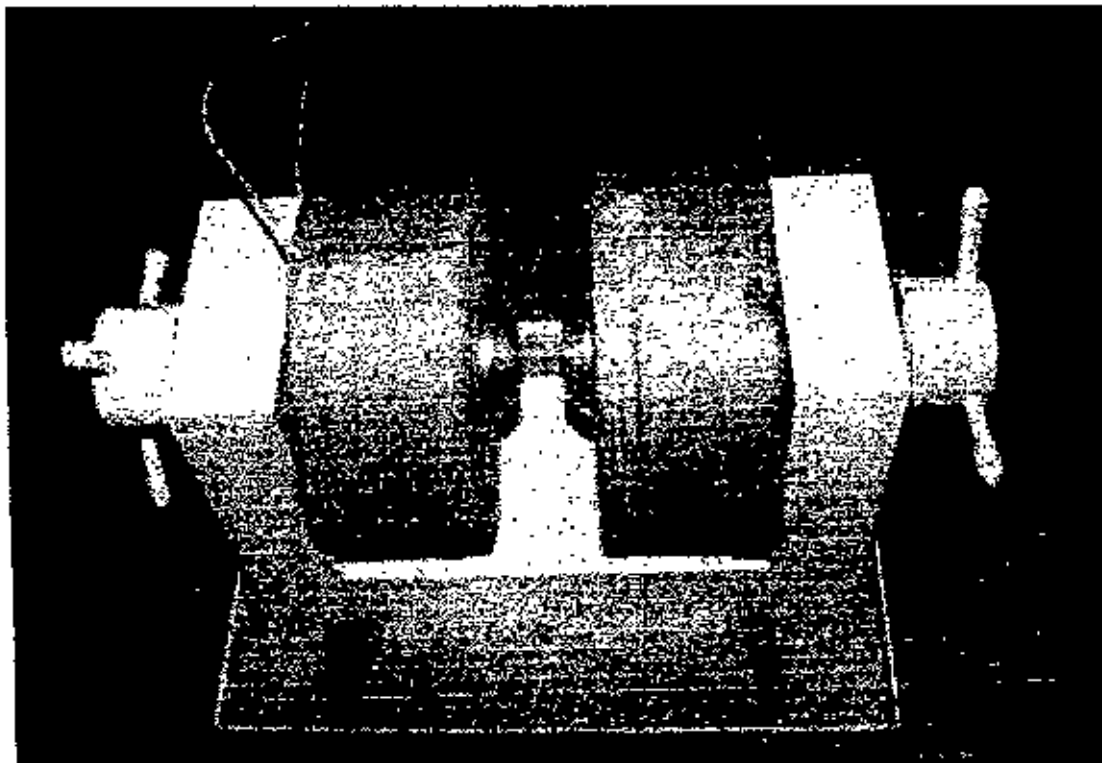


Figure 3.2: Schematic diagram of the Electromagnet.

The major parts of the electromagnets are base pole piece holder, pole pieces and coils. Base of the electromagnet is made up of a parallel piped shaped mild steel bar of dimension $36 \text{ cm} \times 19 \text{ cm} \times 8 \text{ cm}$. Pole piece holder of the electromagnet is also made from commercial mild steel bar. Two pole piece holders are attached to both side of the base with L type bolt. Each pole piece holder is a parallelepiped of dimension $32 \text{ cm} \times 19 \text{ cm} \times 8 \text{ cm}$. Pole pieces (cylindrical soft iron of final diameter 9.2 cm) are attached in these holders in such a way so that we can vary the pole gap. The pole gap may vary from 9.10 cm . As the lower part of our crystal has outer dimension 3.8 cm , pole gap of this size will be suitable for the magnet operation.

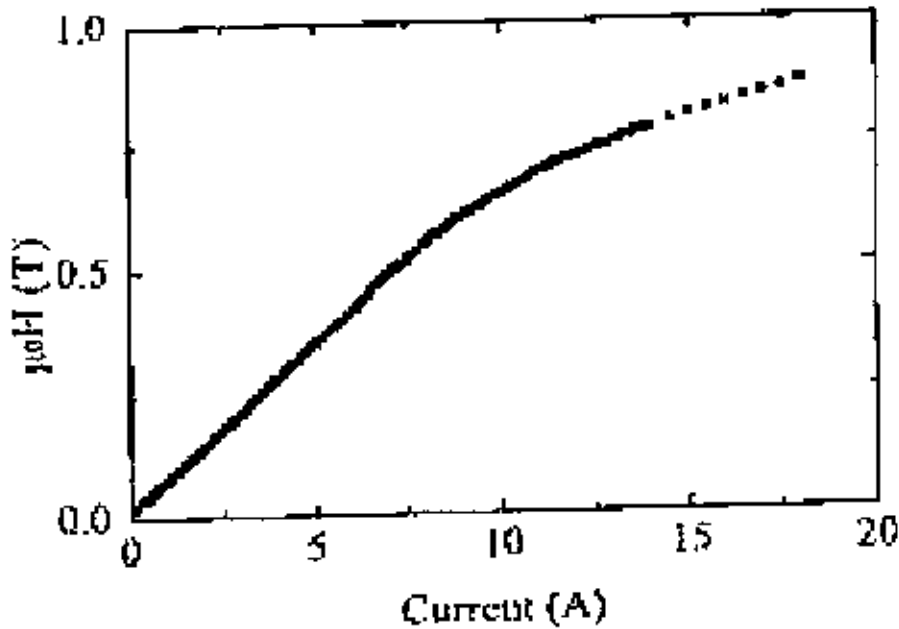


Fig 3.3: calibration of the home made electromagnet.

Two induction coils for two pole-pieces have been made with insulated copper wire of S.W G 14. The length of each coil is 12 cm. The number of turns in each layer of the coil is 58 and total number of layers is 44. So the total number of turns is 2552. The resistance of each coil is about 8 Ω . The weight of each coil is about 40 kg. Two coils are set in the pole pieces of the electromagnet. They are connected in parallel combination with the dc power supply. The calibration curve of the electromagnet is given in figure (3.3). A field of 0.7T was obtained for a current of 18A.

The constructed electromagnet has been tested to know its magnetic field generation capacity with a constant pole-gap 3.8 cm as the outer dimension of the lower part of the crystal is 3.8 cm. The maximum current we have applied to the coils is 18 A. This current generated a dc magnetic field about 0.86 T. Magnetic fields are measured by a Gauss meter. Figure 3.3 shows magnetic field as a function of applied current with a constant pole gap 3.8 cm. The home made cryostat and the electromagnet was assembled together (Figure 3.4) for the magnetoresistance measurement both as a function of temperature (liquid nitrogen temperature to room temperature) and magnetic field.

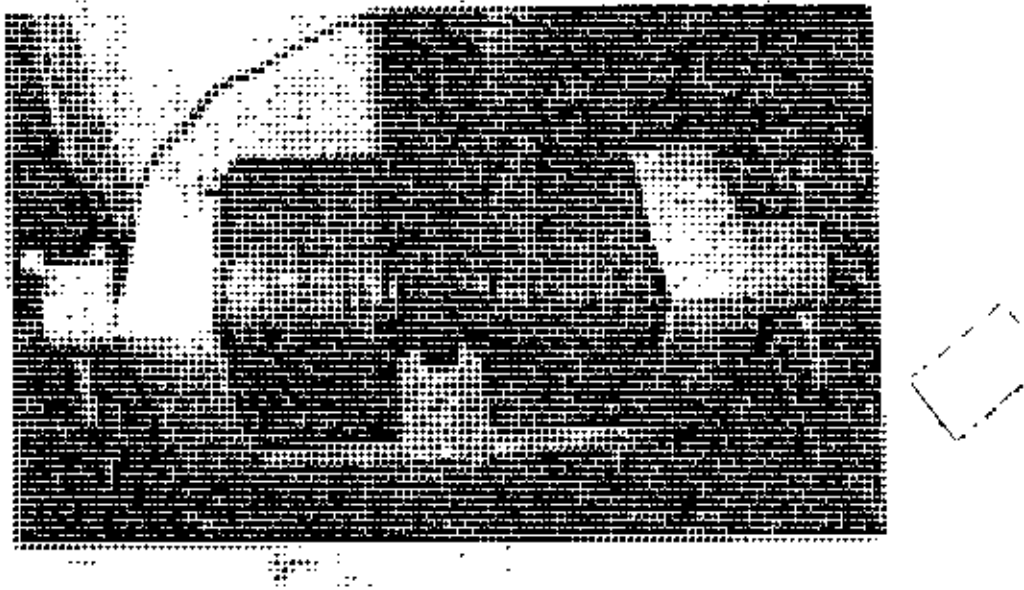


Figure 3.4: Schematic diagram of Magnet and Cryostat Assembly for Magnetoresistance Measurements.

3.8 Construction of the Sample Rod

A sample rod is constructed for four-point resistance measurement. This is a hollow stainless steel tube. The upper part is connected with multipoint connectors and lower part has a copper sample holder as shown in figure. The sample rod is connected with the cryostat by a union socket. A schematic diagram of the sample rod is shown in figure 3.5. The carbon glass resistor used as a temperature sensor is kept in close contact with the specimen. For the magnetoresistance measurements we have to apply magnetic field in the sample space. The carbon glass resistor has a very weak sensitive in the magnetic field.

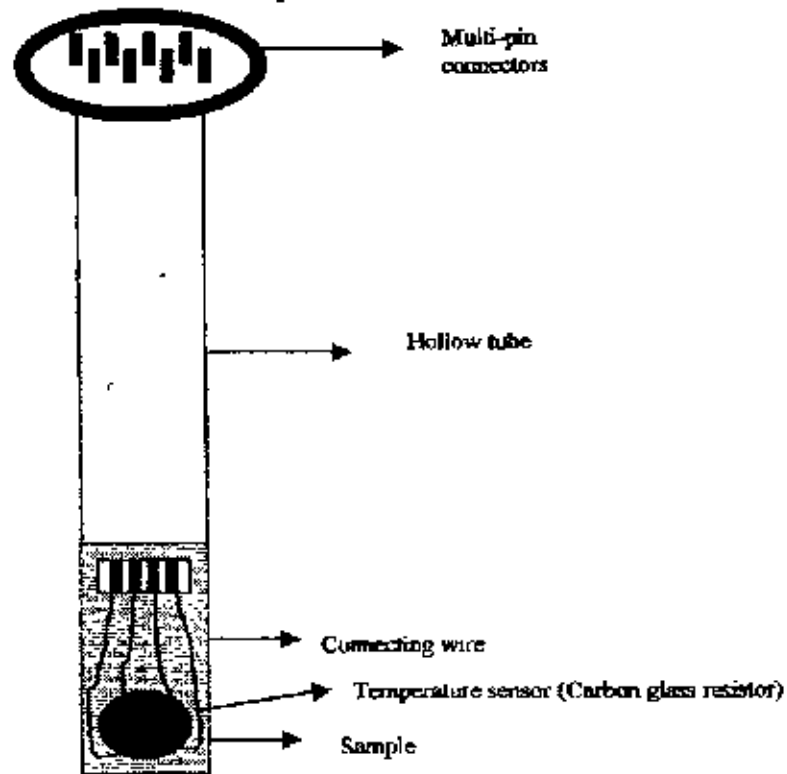


Figure 3.5: Schematic diagram of the sample holder.

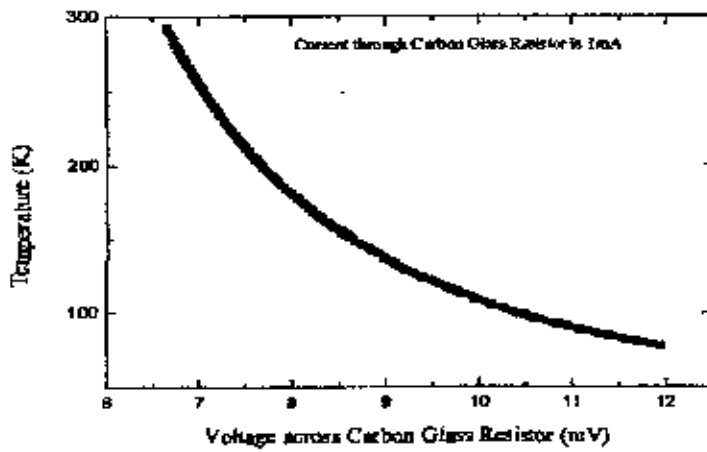


Figure 3.6: Calibration curve of the temperature sensor (Lakeshore carbon Glass resistor).

3.9 Magnetoresistance Measurement Set-up

Figure 3.7 shows the full view of the cryostat used for magnetoresistance measurements.

Figure 3.8 shows the schematic diagram of the Magnetoresistance measurement set up.

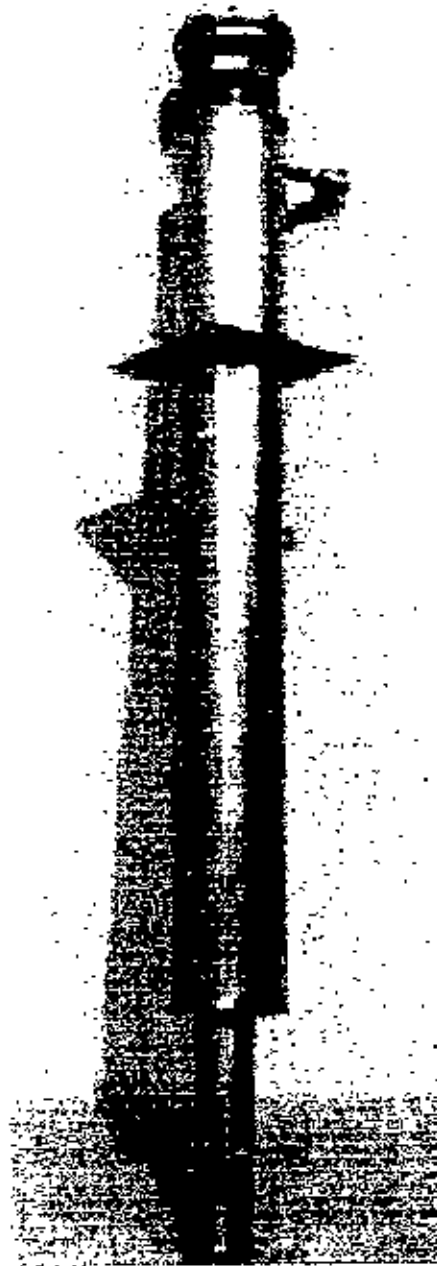


Figure 3.7: A Snapshot of the constructed cryostat.

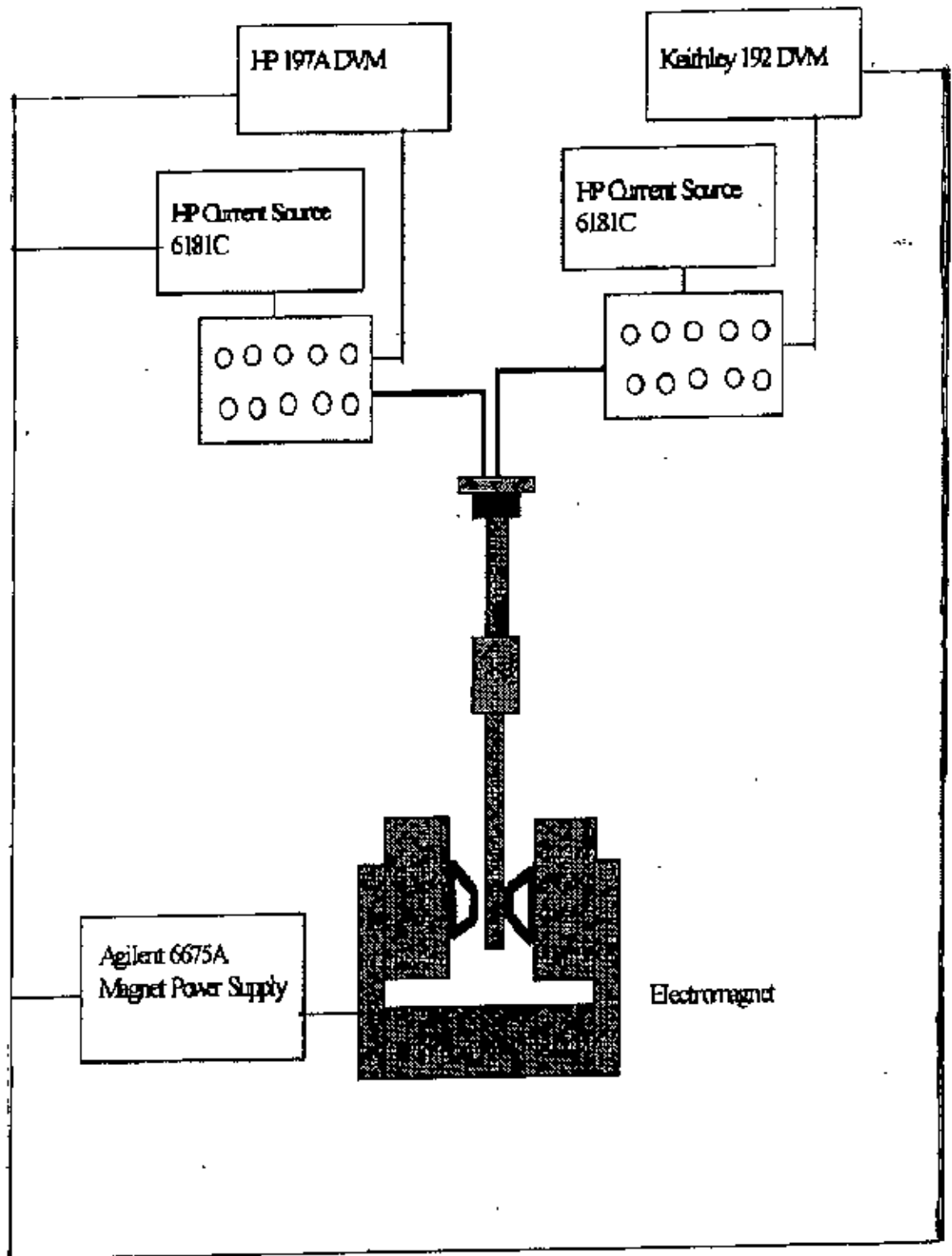


Figure 3.8: Experimental set-up for magnetoresistance measurements.

The standard four point technique was used for resistance measurements.

All samples for test are mounted on the specimen holder and inserted in the sample well of the cryostat. The temperature of the sample is measured with a calibrated carbon-glass resistor placed close to the sample. The thermometer is sourced (1mA) by a HP 6181C constant current source and voltage is measured with Keithly 192 digital voltmeter. The sample current is source with another 6181C constant current source and voltage drop is measure with HP 197A nanovolt meter.

For magnetoresistance measurements, the electromagnet is powered by Agilent 6675A power supply. The system is capable of creating a field up to 0.7T for a current of $\approx 18A$.

3.10 The Van der Pauw Technique

The resistivities of our disc shaped samples were calculated using the Van der Pauw technique [1,2]. This technique is based on four point measurements providing the following conditions are fulfilled.

- (a) The contacts are on the circumference of the sample.
- (b) The contacts are sufficiently small.
- (c) The sample is homogeneous in thickness.
- (d) The surface of the sample is singly connected, i.e. the sample dose not have isolated holes.

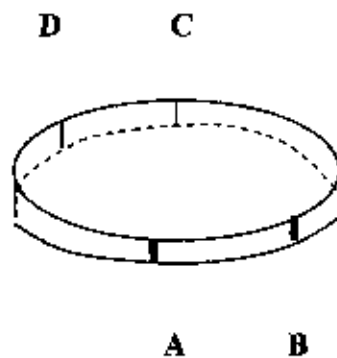


Figure 3.9: The four electrical contacts on the circumference of the disc shaped sample.

Figure 3.9 shows the four contacts on the circumference of the disc shaped sample. For a fixed temperature, we define the resistance $R_{AB, CD}$ as the potential difference between $V_D - V_C$ between the contacts D and C per unit current through the contacts A and B. Similarly, we define $R_{BC, DA}$. Now if the uniform sample thickness is t then according to van der pauw the $\rho(T)$ will be

$$\rho(T) = \frac{\pi t}{\ln 2} \{ (R_{AB, CD} + R_{BC, DA}) / 2 \} f (R_{AB, CD} / R_{BC, DA}) \dots\dots\dots (3.1)$$

$$\rho(T) = \frac{\pi t}{\ln 2} \left(\frac{R_{AB, CD} + R_{BC, DA}}{2} \right) f \left(\frac{R_{BC, DA}}{R_{AB, CD}} \right)$$

Where f is a function of the ratio $R_{AB, CD} / R_{BC, DA}$ only and satisfies the relation

$$(R_{AB, CD} - R_{BC, DA}) / (R_{AB, CD} + R_{BC, DA}) = f \operatorname{arccosh} \{ \exp(\ln 2 / f) / 2 \} \dots\dots\dots (3.2)$$

If we assume $R_{AB, CD} / R_{BC, DA} = Q$, then equation 3.2 becomes

$$(Q - 1) / (Q + 1) = f \operatorname{arccosh} \{ \exp(\ln 2 / f) / 2 \}$$

A plot of this function is shown in figure 3.10.

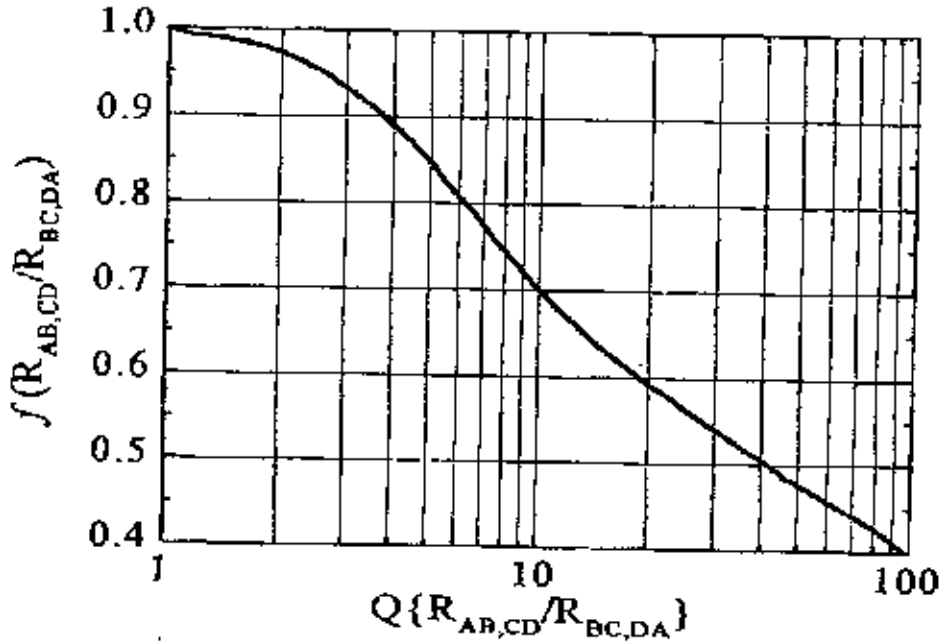


Figure 3.10: the function $f(Q)$ for determining the resistivity of the sample (From ref [3])

In practice the electrical contacts have finite dimension. Van der Pauw showed that if one of the contacts is of finite length l and is assumed that it lies along the circumference of the sample of diameter D then

$$\Delta \rho / \rho \approx -l^2 / 16 D^2 \ln 2$$

Also, if all contacts have similar defects the errors introduced are additive. Our sintered disc shaped sample has a diameter $\sim 11\text{mm}$ and if we assume the maximum width dimensions of the contacts are 1mm then the errors introduced into our measurement due to finite sized contacts will be 0.3% . In fact we have used $5\mu\text{m}$ silver paint for the contacts which are much smaller than 1mm .

3.11 Magnetoresistance

The R(T) data was acquired both in zero field and in the presence of field. The R(T) data was converted to $\rho(T)$ using the Van der Pauw expression. The magnetoresistance (MR), which is a function of field and temperature, was calculated using the following expression

$$MR(T,H)\% = -\frac{\rho(T,0)-\rho(T,H)}{\rho(T,0)} \times 100 \quad (3.5)$$

References:

- [1] L.J Van der Pauw , "A method of measuring specific resistivity and Hall effects of discs of arbitrary shape," *Philips Research Reports* 13[1], 1-9 (1958).
- [2] L.J Van der Pauw , "A method of measuring specific the resistivity and Hall coefficient on lamellae of arbitrary shape," *Philips Technical Review* 20[8] 220-224 (1958/59).
- [3] Keithley, Low Level Measurements, 4th Edition ed. (Keithly Instruments,Inc., 1992)

Chapter-4

Results & Discussions

The various polycrystalline $(La_{2-x}Ho_x)(Ba_{1-y}Ca_y)Mn_2O_7$ (where $x=0.0,0.1,0.2$ & $y=0.0,0.1,0.2$) samples were sintered at 1100°C . X-ray diffraction was carried out on the powder samples. The result of DC electrical measurements including magnetic phase transitions, resistivity and magnetoresistance as a function of applied magnetic field and temperature (both at room temperature and liquid nitrogen temperature) were reported.

4.1 X-ray diffraction analysis

To characterize the samples, X-ray diffraction analysis was carried out with a X-ray diffractometer using $M_o K_\alpha$ radiation ($\lambda=0.709\text{\AA}$). X-ray diffraction analysis did not reveal any inclusions of unreacted components in the target, suggesting that the samples were homogeneous in chemical compositions. Figure 4.1 shows the X-ray diffraction patterns for the polycrystalline samples of the series $(La_{2-x}Ho_x)(Ba_{1-y}Ca_y)Mn_2O_7$ (Where $x=0.0, 0.1, 0.2$ & $y=0.0, 0.1, 0.2$). Table 4.1 gives the comparative peak positions observed for these samples. The observed positions of the diffraction peaks are almost in identical position and thus confirmed the single-phase perovskite structure with no significant trace of impurity.

Table 4.1: X-ray diffraction peak positions for various polycrystalline samples

Sample composition	X-ray peak position 2θ (degree)							
	1st	2nd	3rd	4th	5th	6th	7th	8th
$La_2BaMn_2O_7$	14.3	17.4	20.3	25.1	29.2	32.7	39	44.6
$La_{1.9}Ho_{0.1}BaMn_2O_7$	14.4	17.6	20.4	25.3	29.3	33	39.3	45
$La_{1.8}Ho_{0.2}BaMn_2O_7$	14.2	17.5	20.4	25.1	29.2	32.7	39.3	45
$La_2Ba_{0.9}Ca_{0.1}Mn_2O_7$	14.3	17.6	20.4	25.2	29.3	32.8	39	44.9
$La_2Ba_{0.8}Ca_{0.2}Mn_2O_7$	14.3	17.8	20.6	25.2	29.2	33	39	45
$La_{1.9}Ho_{0.1}Ba_{0.8}Ca_{0.2}Mn_2O_7$	14.3	17.4	20.4	25	29	32.6	39	44.5
$La_{1.8}Ho_{0.2}Ba_{0.9}Ca_{0.1}Mn_2O_7$	14.3	17.8	20.3	25.2	29.2	33.7	39.2	44.5

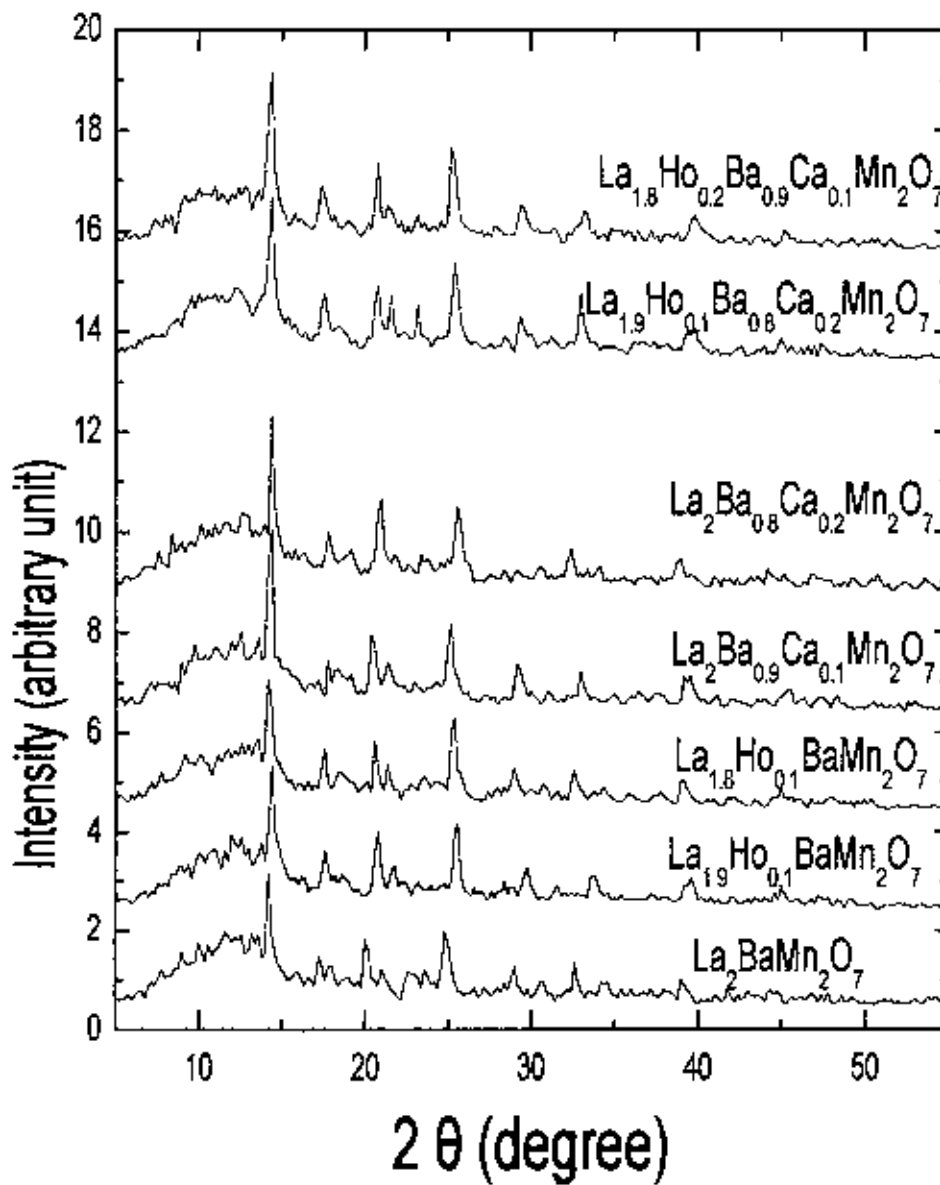


Figure 4.1: X-ray diffraction patterns of various polycrystalline samples

4.2 DC Electrical Resistivity

4.2.1 DC Electrical Resistivity of $\text{La}_{2-x}\text{Ho}_x\text{BaMn}_2\text{O}_7$

The temperature dependence of normalized resistivity, $\rho(T)/\rho(RT)$, where RT is room temperature, at zero applied magnetic field for various $\text{La}_{2-x}\text{Ho}_x\text{BaMn}_2\text{O}_7$ (where $x=0.0, 0.1, 0.2$) polycrystalline samples sintered at 1100°C in air are shown in Figure 4.2. Figure 4.3 shows the corresponding behavior of these samples in presence of 0.7T applied magnetic field. From figure 4.2 & 4.3 it is evident that all the samples show a metal insulator (M-I) transition at temperature T_p . The M-I transition temperature decreases when La is replaced by Ho. It is well-known that the substitution of the lanthanide ions by some other ions in the perovskite significantly modifies the structural and magnetic properties. The atomic size of Ho (1.02 \AA) is lower than that of La (1.18 \AA) For the different atomic sizes of the doping elements the crystal structure would be distorted due to Jahn-Teller effect and changes would arise in the transition peak. Previous investigation showed that [1] any deviation from the ideal cubic structure can lead to either a reduction in the Mn-O-Mn bond angle from 180° , or bond length directly affecting the double exchange. Therefore, the result of replacing La by Ho is found to lower the ferromagnetic transition temperature. All the samples show the ferromagnetic metallic characteristics ($d\rho/dT > 0$) below phase transition temperature T_p and paramagnetic insulating characteristics ($d\rho/dT < 0$) above the phase transition temperature T_p . The transition temperature T_p for various samples both with zero applied magnetic field and 0.7T applied magnetic field are shown in table 4.2. This sort of M-I transition can be described within the framework of lattice mismatch. Previous investigations by various researchers indicate that the metal-insulator transition temperature in these manganites are generally very close to the Curie temperature T_c , the paramagnetic to ferromagnetic transition temperature.

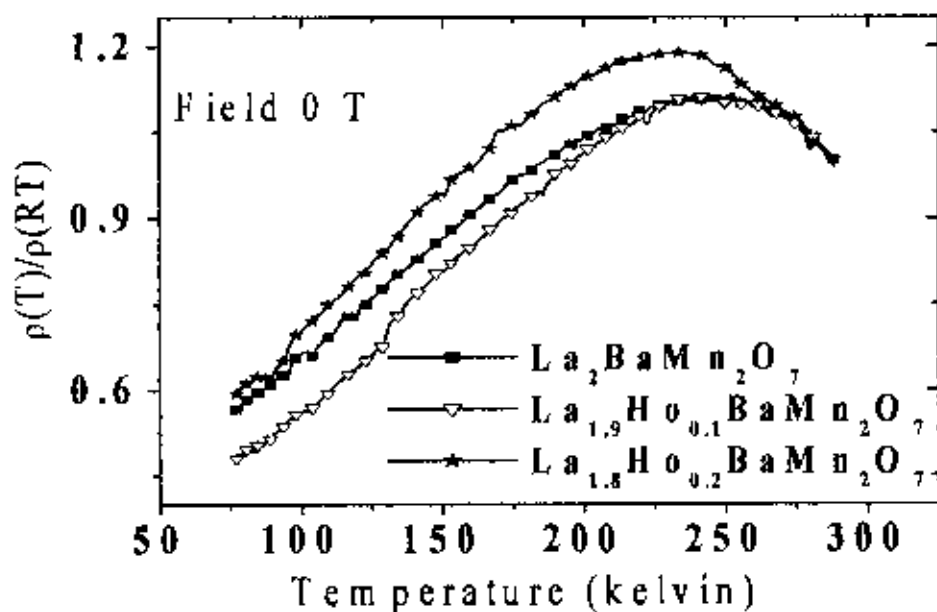


Figure 4.2: The zero field normalized resistivity as a function of temperature for various $\text{La}_{2-x}\text{Ho}_x\text{BaMn}_2\text{O}_7$ (where $x=0.0,0.1,0.2$) polycrystalline samples sintered at 1100°C in air.

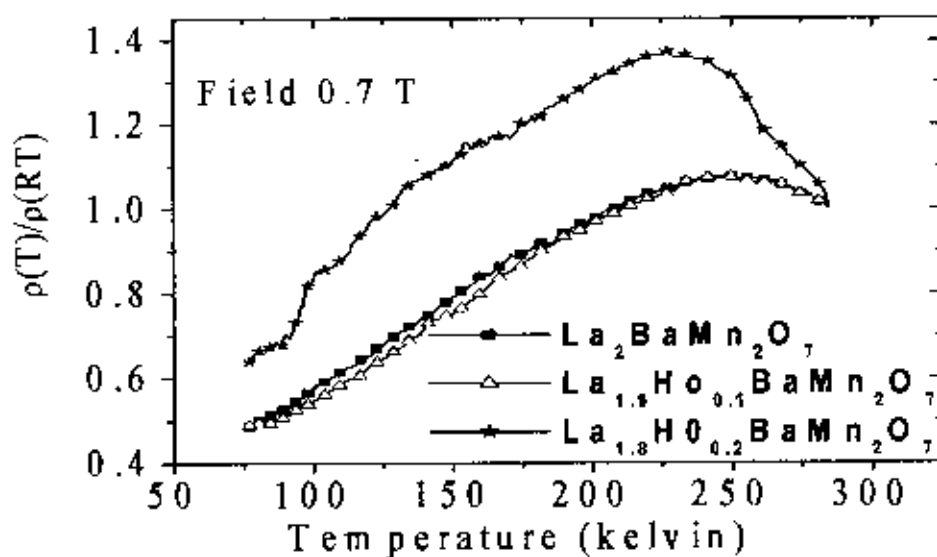


Figure 4.3: The normalized resistivity with constant magnetic field 0.7T as a function of temperature for various $\text{La}_{2-x}\text{Ho}_x\text{BaMn}_2\text{O}_7$ (where $x=0.0,0.1,0.2$) polycrystalline samples sintered at 1100°C in air.

Table 4.2: The metal-insulator transition temperatures T_p for $H=0T$ & $H=0.7T$ for various $(La_{2-x}Ho_x)(Ba_{1-y}Ca_y)Mn_2O_7$ polycrystalline samples

Sample Composition	Sintering Temperature	T_p (K)	
		$H=0T$	$H=0.7T$
$La_2BaMn_2O_7$	1100° C	248	250
$La_{1.9}Ho_{0.1}BaMn_2O_7$		245	248
$La_{1.8}Ho_{0.2}BaMn_2O_7$		230	232
$La_2Ba_{0.9}Ca_{0.1}Mn_2O_7$		190	192
$La_2Ba_{0.8}Ca_{0.2}Mn_2O_7$		99	100
$La_{1.9}Ho_{0.1}Ba_{0.8}Ca_{0.2}Mn_2O_7$		118	119
$La_{1.8}Ho_{0.2}Ba_{0.9}Ca_{0.1}Mn_2O_7$		250	254

The others point of consideration is that the resistivity of FM metal has a quite pronounced contribution from the electron scattering on spin disorder (apart from the usual contribution from crystal lattice defects and electron-phonon scattering). Higher number of electrons result other types of interactions, spin fluctuations which gives rise to increase further spin disorder in the compound. The presence of 0.7T magnetic field in this investigation increases M-I transition temperature only by few Kelvin. This means that the applied field is not sufficient for the suppression of spin fluctuations.

4.2.2. DC Electrical Resistivity of $La_2Ba_{1-y}Ca_yMn_2O_7$

The temperature dependence of normalized resistivity, $\rho(T)/\rho(RT)$, where RT is room temperature at zero applied magnetic field for the samples $La_2Ba_{1-y}Ca_yMn_2O_7$ ($y=0.1,0.2$) sintered at 1100°C in air shown in Figure 4.4 Figure 4.5 shows the corresponding behavior of the samples in presence of 0.7T applied magnetic field. From the ρ -T curve it is clear that these samples also show M-I transition both in zero applied magnetic fields and 0.7T applied magnetic field. The reasons for such type of transition is again is the lattice distortion which was described in section 4.2.1 for

$\text{La}_{2-x}\text{Ho}_x\text{BaMn}_2\text{O}_7$ samples. But the results of Ca doping in place of Ba causes a large change on phase transition temperature. In samples $\text{La}_2\text{Ba}_{1-y}\text{Ca}_y\text{Mn}_2\text{O}_7$ ($y = 0.1$ and 0.2) the Mn ions are occupying B sites and are surrounded by oxygen octahedra and La, Ba and Ca cations are in the A site. For a perfect cubic structure, the Mn-O-Mn bond angle is equal to 180° and undistorted MnO_6 octahedra are forming a rigid three-dimensional network. Upon substitution of Ba (atomic radius $\sim 1.35 \text{ \AA}$) with Ca which has a smaller atomic radius ($\sim 1.00 \text{ \AA}$), the MnO_6 octahedra are forced to distort in order to compensate the resulting variation of space around A site. This distortion of MnO_6 octahedra lowers the Mn-O-Mn bond angle and thus reduces M-I transition temperature. Thus the doping of Ca in place of Ba results a lower of ferromagnetic transition temperature.

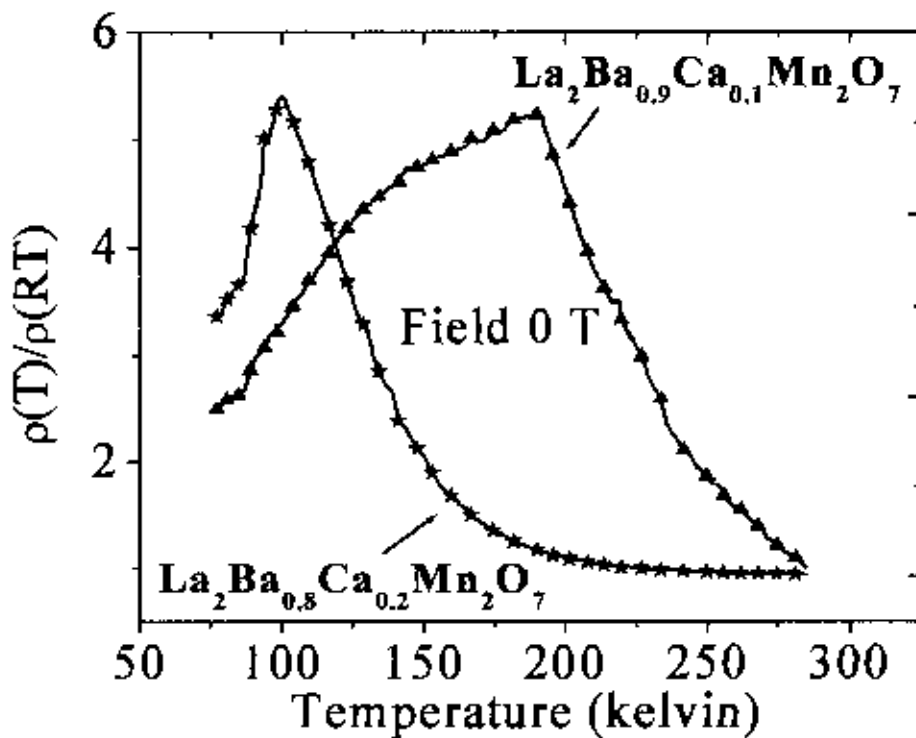


Figure 4.4: The zero field normalized resistivity as a function of temperature for various $\text{La}_2\text{Ba}_{1-y}\text{Ca}_y\text{Mn}_2\text{O}_7$ (where $y=0.1, 0.2$) polycrystalline samples sintered at 1100°C in air.

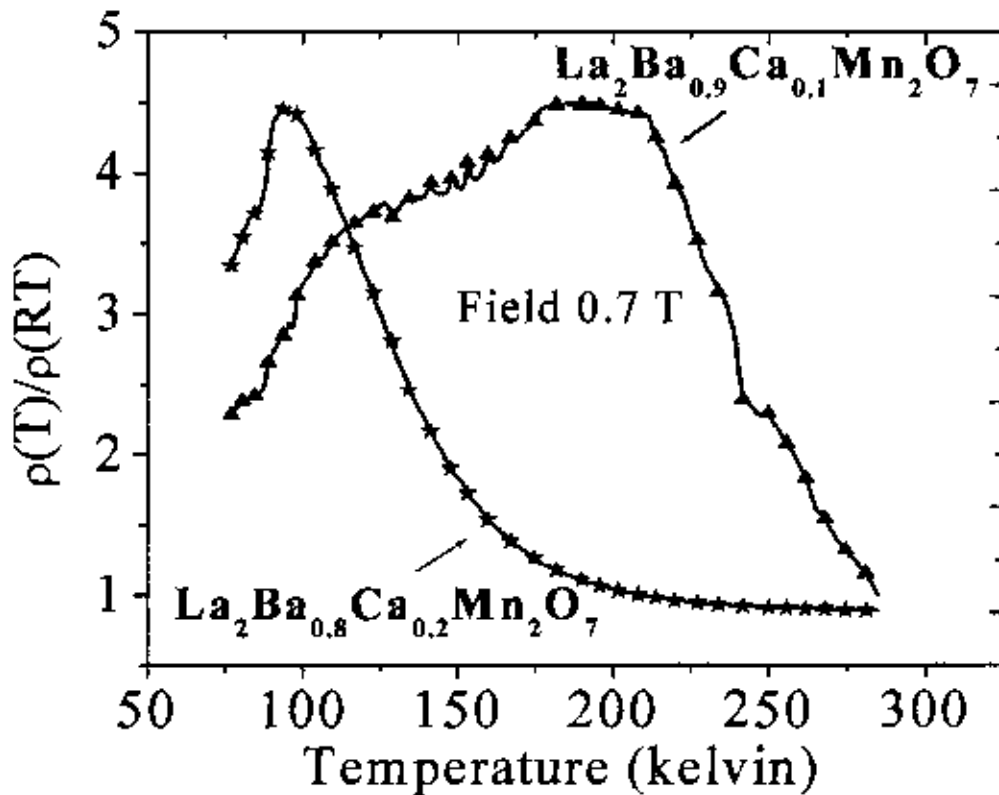


Figure 4.5 The normalized resistivity with constant magnetic field 0.7 T as a function of temperature for various $\text{La}_2\text{Ba}_{1-y}\text{Ca}_y\text{Mn}_2\text{O}_7$ (where $y=0.1, 0.2$) polycrystalline samples sintered at 1100°C in air

4.2.3 DC Electrical Resistivity of $\text{La}_{1.9}\text{Ho}_{0.1}\text{BaMn}_2\text{O}_7$ & $\text{La}_{1.9}\text{Ho}_{0.1}\text{Ba}_{0.8}\text{Ca}_{0.2}\text{Mn}_2\text{O}_7$

In figure 4.6 the normalized resistivity, $\rho(T)/\rho(RT)$, where RT is room temperature at zero applied magnetic field for $\text{La}_{1.9}\text{Ho}_{0.1}\text{BaMn}_2\text{O}_7$ & $\text{La}_{1.9}\text{Ho}_{0.1}\text{Ba}_{0.8}\text{Ca}_{0.2}\text{Mn}_2\text{O}_7$ polycrystalline samples sintered at 1100°C in air is shown. Figure 4.7 shows the corresponding behavior of these samples in presence of 0.7 T applied magnetic field. The samples $\text{La}_{1.9}\text{Ho}_{0.1}\text{BaMn}_2\text{O}_7$ & $\text{La}_{1.9}\text{Ho}_{0.1}\text{Ba}_{0.8}\text{Ca}_{0.2}\text{Mn}_2\text{O}_7$ also show a metal-insulator transition at temperature 245 K and 118 K respectively. So it is obvious that the transition temperature again decreases upon the substitution of Ca in place of Ba. The observation is in consistent with the previous observations. The result of 0.7 T applied magnetic field in these two samples also the enhancement of the transition temperature only by few

Kelvin. Near the transition temperature the spin system is almost insensitive to external field and does not cause a change of the local spin disorder and thereby of the carrier mobility.

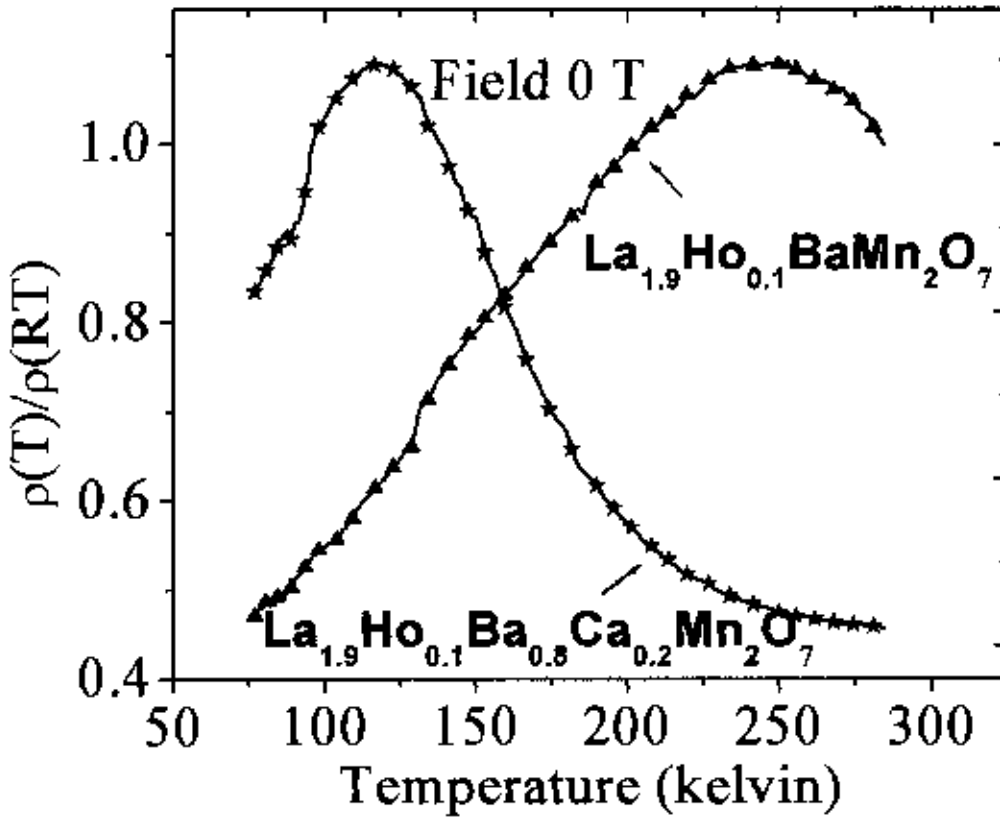


Figure 4.6: The zero field normalized resistivity as a function of temperature for various $\text{La}_{1.9}\text{Ho}_{0.1}\text{BaMn}_2\text{O}_7$ & $\text{La}_{1.9}\text{Ho}_{0.1}\text{Ba}_{0.8}\text{Ca}_{0.2}\text{Mn}_2\text{O}_7$ polycrystalline samples sintered at 1100°C in air.

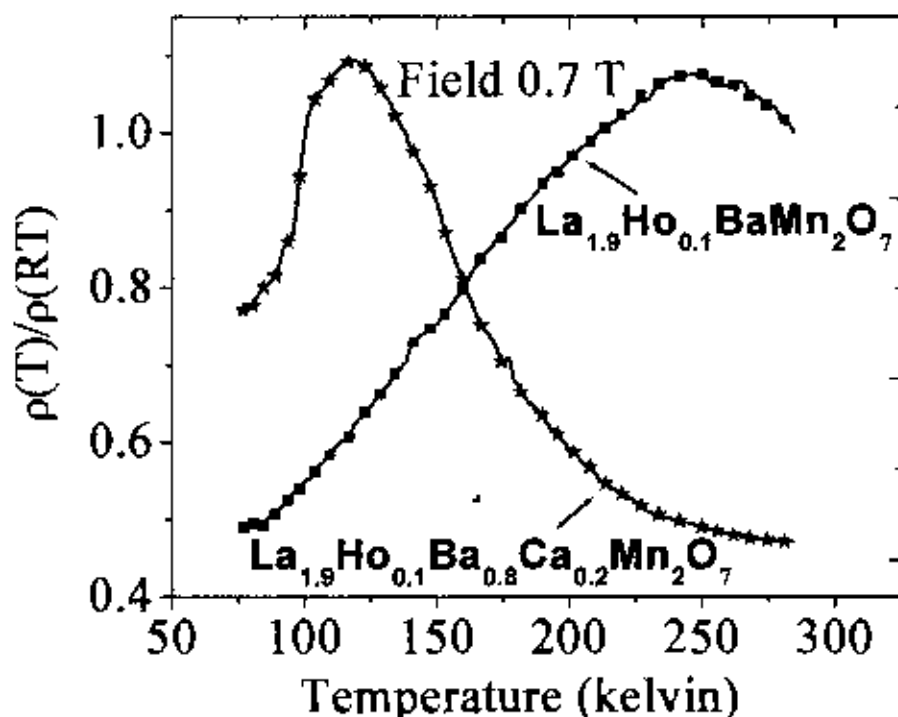


Figure 4.7: The normalized resistivity with constant magnetic field 0.7T as a function of temperature for various $\text{La}_{1.9}\text{Ho}_{0.1}\text{BaMn}_2\text{O}_7$ & $\text{La}_{1.9}\text{Ho}_{0.1}\text{Ba}_{0.8}\text{Ca}_{0.2}\text{Mn}_2\text{O}_7$ polycrystalline samples sintered at 1100°C in air.

4.2.4 DC Electrical Resistivity of $\text{La}_{1.8}\text{Ho}_{0.2}\text{BaMn}_2\text{O}_7$ & $\text{La}_{1.8}\text{Ho}_{0.2}\text{Ba}_{0.9}\text{Ca}_{0.1}\text{Mn}_2\text{O}_7$

Figure 4.8 and 4.9 shows the temperature dependence normalized resistivity behavior for samples $\text{La}_{1.8}\text{Ho}_{0.2}\text{BaMn}_2\text{O}_7$ & $\text{La}_{1.8}\text{Ho}_{0.2}\text{Ba}_{0.9}\text{Ca}_{0.1}\text{Mn}_2\text{O}_7$ at zero applied magnetic field and 0.7T applied magnetic field, respectively. From the ρ -T curve for these two samples it is observed that the transition temperature is increased upon the substitution of small amount of Ca in place of Ba, an anomalous behavior with respect to the previous observations. But 0.7T applied magnetic field in these two samples causes the transition temperature enhanced only by few Kelvin.

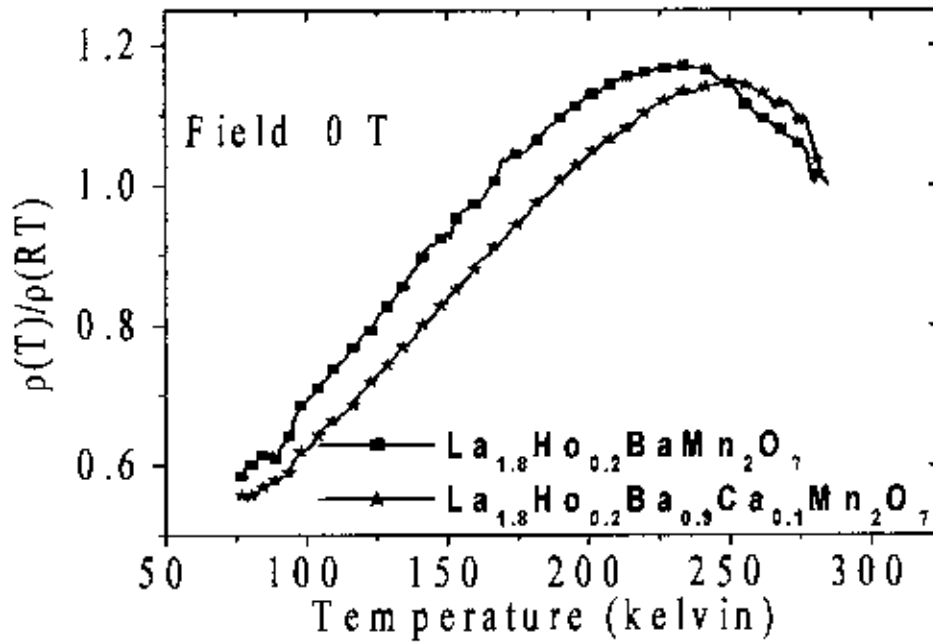


Figure 4.8: The zero field normalized resistivity as a function of temperature for various $\text{La}_{1.8}\text{Ho}_{0.2}\text{BaMn}_2\text{O}_7$ & $\text{La}_{1.8}\text{Ho}_{0.2}\text{Ba}_{0.9}\text{Ca}_{0.1}\text{Mn}_2\text{O}_7$ polycrystalline samples sintered at 1100°C in air.

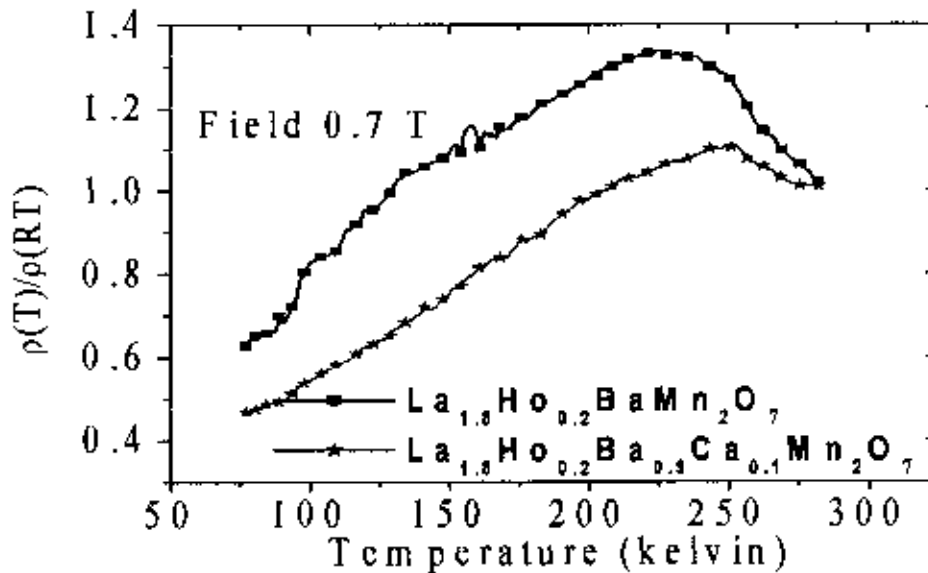


Figure 4.9: The normalized resistivity with constant magnetic field 0.7T as a function of temperature for various $\text{La}_{1.8}\text{Ho}_{0.2}\text{BaMn}_2\text{O}_7$ & $\text{La}_{1.8}\text{Ho}_{0.2}\text{Ba}_{0.9}\text{Ca}_{0.1}\text{Mn}_2\text{O}_7$ polycrystalline samples sintered at 1100°C in air

4.3 Magnetoresistance

The Magnetoresistance (MR) as a function of magnetic field of the samples was measured at room temperature and liquid nitrogen temperature. The MR was calculated using following formula.

$$MR \% = \frac{\rho(H) - \rho(H = 0)}{\rho(H = 0)} \times 100$$

For the magnetoresistance measurement the magnetic field was applied perpendicularly to the surface of the samples.

4.3.1 Magnetoresistance of various polycrystalline samples:

The magnetoresistance (MR) as a function of magnetic field for various polycrystalline samples ($\text{La}_{2-x}\text{Ho}_x$) ($\text{Ba}_{1-y}\text{Ca}_y$) Mn_2O_7 sintered at 1100°C was measured both at room temperature and liquid nitrogen temperature. Figure 4.10 show the MR as a function of magnetic field at room temperature. The observed MR is almost linear with the applied magnetic field for various x & y values. In the present investigation the polycrystalline sample $\text{La}_2\text{BaMn}_2\text{O}_7$ shows 4.7% MR at room temperature. Whereas samples $\text{La}_{1.9}\text{Ho}_{0.1}\text{BaMn}_2\text{O}_7$ and $\text{La}_{1.8}\text{Ho}_{0.2}\text{BaMn}_2\text{O}_7$ show 4.3% MR. at RT. The result of MR curves are summarized in Table 4.3.

The MR at 78 K for various polycrystalline samples sintered at 1100°C are shown in figure 4.11. A large change MR is observed in the presence of low applied magnetic field. For sample $\text{La}_2\text{BaMn}_2\text{O}_7$ the total change of MR is 17% under the application of 860mT magnetic field. Out of this amount of MR%, 15% change occurs upon the application of 225 mT magnetic field. The other samples also show similar behavior i.e. a sharp drop of MR at low magnetic field.

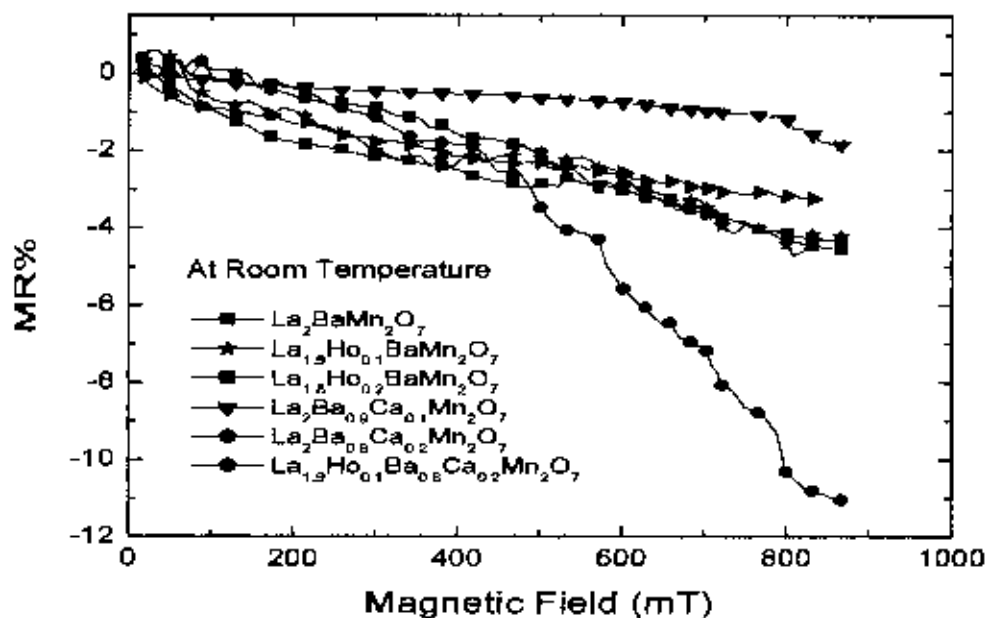


Figure 4.10: Variation of MR with applied magnetic field at room temperature for various polycrystalline samples

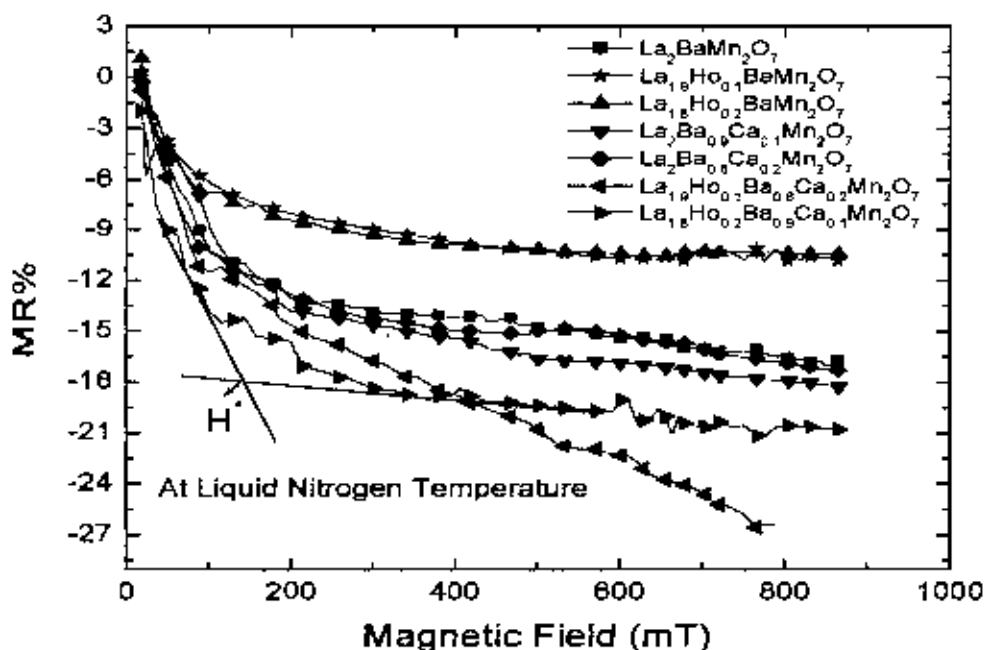


Figure 4.11: Variation of MR with applied magnetic field at 78K for various polycrystalline samples

Table 4.3: The % MR curve for various polycrystalline samples.

Sample composition	Sintering Condition	MR at RT(%)	MR at 77 K(%)
$\text{La}_2\text{BaMn}_2\text{O}_7$	1100°C	4.73	17.118
$\text{La}_{1.9}\text{Ho}_{0.1}\text{BaMn}_2\text{O}_7$..	4.31	10.42
$\text{La}_{1.8}\text{Ho}_{0.2}\text{BaMn}_2\text{O}_7$..	4.31	10.42
$\text{La}_2\text{Ba}_{0.9}\text{Ca}_{0.1}\text{Mn}_2\text{O}_7$..	1.83	17.27
$\text{La}_2\text{Ba}_{0.8}\text{Ca}_{0.2}\text{Mn}_2\text{O}_7$..	11.03	18.18
$\text{La}_{1.9}\text{Ho}_{0.1}\text{Ba}_{0.8}\text{Ca}_{0.2}\text{Mn}_2\text{O}_7$..	1.9	27
$\text{La}_{1.8}\text{Ho}_{0.2}\text{Ba}_{0.9}\text{Ca}_{0.1}\text{Mn}_2\text{O}_7$..	-	20.75

So, the MR behavior of the polycrystalline samples of the present investigation can be characterized by two features: 1) a sharp increase of magnetoresistance at low fields followed by 2) a linear dependence at higher fields. This may be due to the reason that as the materials are subdivided into domains, low field was quite sufficient to align the domain spins and thus a sharp decrease in MR was observed but to align the spins at the domain boundary requires much larger field leading to weak field dependence. It has been suggested by Gupta et al.,[2] and Li et al.,[3] that the low-field magnetoresistance, which is consistently observed in polycrystalline manganites, is due to spin-dependent scattering in grain boundaries. Evetts et al.[4] suggested that the high-field magnetoresistance is associated with a magnetically mesoscopic disordered interface layer present in the vicinity of grain boundaries. This field dependent MR behavior can be explained with the help of the following diagram.

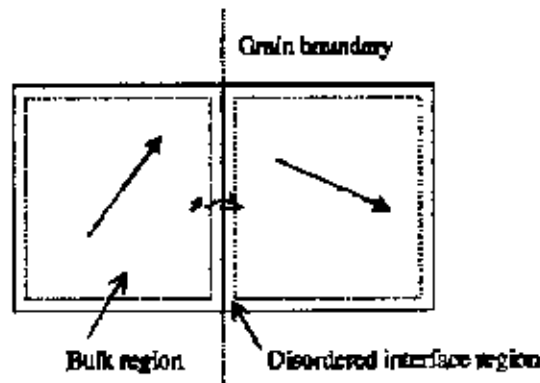


Figure 4.12: Schematic illustration of grain-boundary transport in a polycrystalline mixed-valence manganite. Each grain constitutes a single-magnetic domain. The conduction electrons show a high degree of spin polarization inside the grains. When traveling across the grain boundary conduction electrons may be subject to a strong spin-dependent scattering, which can be reduced if a low external magnetic field aligns the magnetizations of the two grains. Spin alignment in the disordered surface layers gives rise to high-field magnetoresistance.

4.4 Activation energy

Activation energy for the present investigated polycrystalline samples can be calculate from the slopes of straight lines using the relation

$$\rho = \rho_0 \exp(E_0/K_B T)$$

where, E_0 is the activation energy and K_B is the Boltzmann constant

In figure 4.13, $\ln \rho(T)/\rho(RT)$ is plotted against $1/T$ for various polycrystalline samples at sintering temperature 1100°C and applied magnetic field 0T and 0.7T . Table 4.4 shows the values of the activation energies.

All the samples show very good linear behavior in the $\ln \rho(T)/\rho(RT)-T^{-1}$ plots which suggest that conduction occurs through a thermally activated process.

Table 4.4: Activation energy (meV) of the various polycrystalline samples.

Sample Composition	Activation energy (meV)	
	Applied Magnetic Field (0T)	Applied Magnetic Field (0.7T)
$\text{La}_2\text{BaMn}_2\text{O}_7$	21.44	16.22
$\text{La}_{1.9}\text{Ho}_{0.1}\text{BaMn}_2\text{O}_7$	21.52	17.85
$\text{La}_{1.8}\text{Ho}_{0.2}\text{BaMn}_2\text{O}_7$	21.62	18.07
$\text{La}_2\text{Ba}_{0.9}\text{Ca}_{0.1}\text{Mn}_2\text{O}_7$	59.48	58.10
$\text{La}_2\text{Ba}_{0.8}\text{Ca}_{0.2}\text{Mn}_2\text{O}_7$	26.10	23.32
$\text{La}_{1.9}\text{Ho}_{0.1}\text{Ba}_{0.8}\text{Ca}_{0.2}\text{Mn}_2\text{O}_7$	26.45	23.74
$\text{La}_{1.8}\text{Ho}_{0.2}\text{Ba}_{0.9}\text{Ca}_{0.1}\text{Mn}_2\text{O}_7$	29.03	23.90

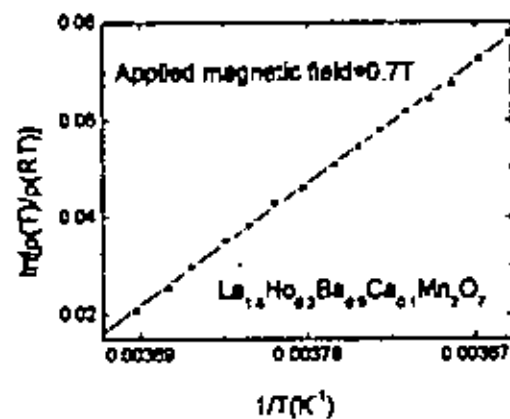
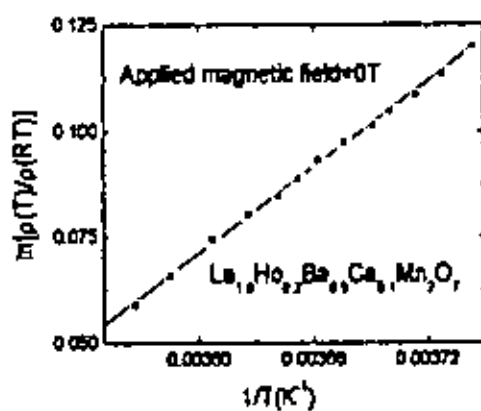


Figure 4.13 (a): $\ln[\rho(T)/\rho(RT)]$ is plotted against $1/T(\text{K}^{-1})$ for various polycrystalline samples at 1100°C sintering temperature

☆

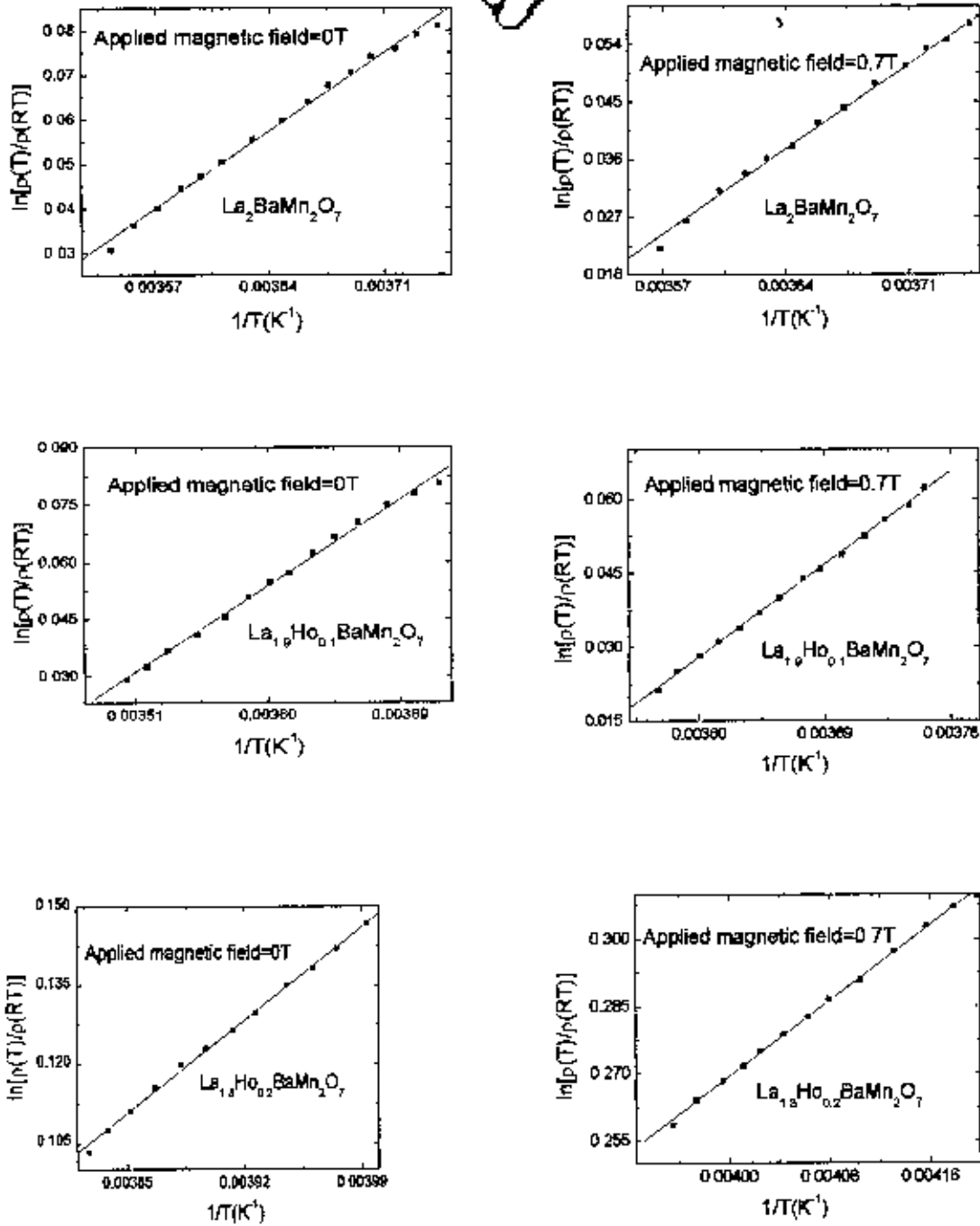
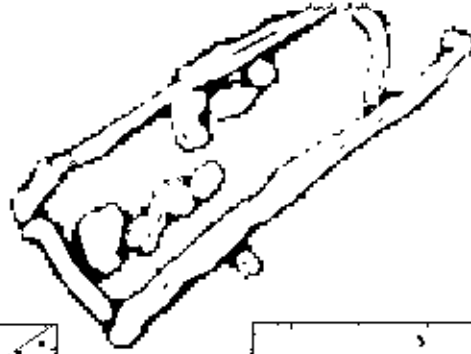


Figure 4.13(b): $\ln[\rho(T)/\rho(RT)]$ is plotted against $1/T(K^{-1})$ for various polycrystalline samples at 1100°C sintering temperature

10/025

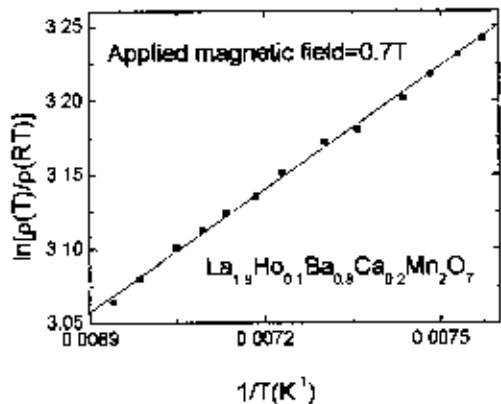
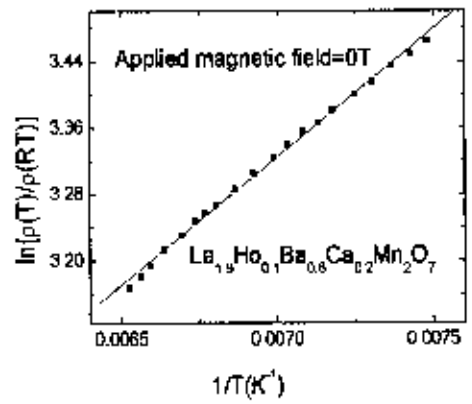
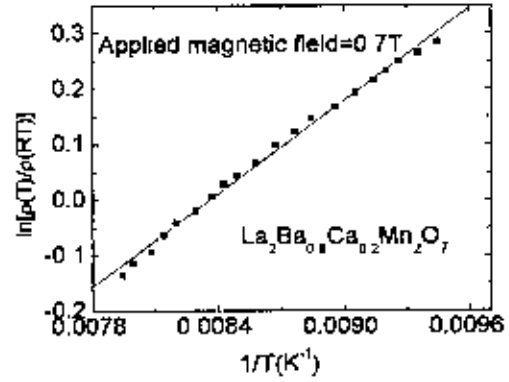
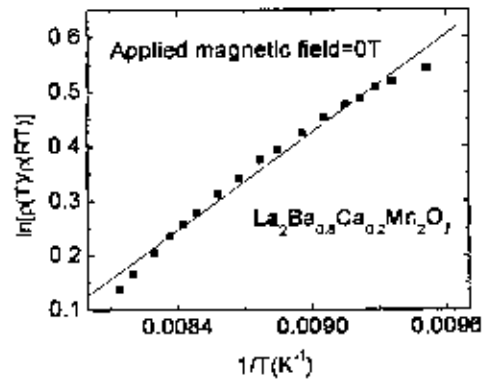
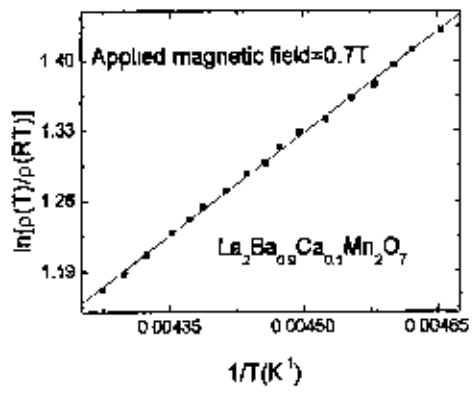
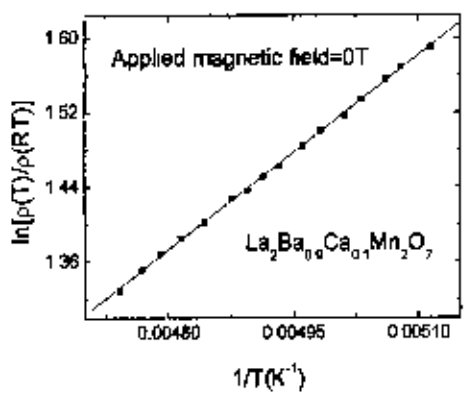


Figure 4.13 (c): $\ln[\rho(T)/\rho(RT)]$ is plotted against $1/T$ (K^{-1}) for various polycrystalline samples at 1100°C sintering temperature

Chapter 4 Results & Discussions

The activation energies obtained from the slopes of the linear curves showed that it increases with the increase of concentration x & y in $\text{La}_{2-x}\text{Ho}_x\text{Ba}_{1-y}\text{Ca}_y\text{Mn}_2\text{O}_7$ polycrystalline samples. It was also observed that the activation energies increases slightly with the substitution of Ho & Ca in place of La & Ba respectively and this is due to the lower sizes of Ho & Ca atom. The result is in agreement with that obtained by A Barman et al [5] for $\text{Pr}_{0.7}\text{R}_{0.1}\text{Ca}_{0.2}\text{MnO}_3$ (R=Y, Dy, Gd, Sm, Nd) samples.

References:

- [1] Ahn K.H., Wu X.W., Liu K., and Chen C.L., "Magnetic properties and colossal magnetoresistance of La(Ca)MnO₃ materials doped with Fe", *Phys.Rev.B*, **54** 15 299 (1996).
- [2] Gupta, A., G. Q. Gong, G. Xiao, P. R. Duncombe, P. Lecoeur, P. Trouilloud, Y. Y. Wang, V. P. Dravid, and J. Z. Sun, "Grain-boundary effects on the magnetoresistance properties of perovskite manganite films", *Phys. Rev. B*, **54** (22), R15629 (1996).
- [3] Li X. W., Gupta A., Xiao G., Gong G. Q., and Gong G. Q., "Low-field magnetoresistive properties of polycrystalline and epitaxial perovskite manganite films", *Appl. Phys. Lett.*, **71** (8), 1124 (1997).
- [4] Everts, J. E., Blamire M. G., Mathur N. D, Isaac S. P., Teo B., Cohen L. F., and Macmanus-Driscoll J. L., "Defect-induced spin disorder and magnetoresistance in single-crystal and polycrystal rare-earth manganite thin film", *Philosophical Transactions of the Royal Society London A*, **356**, 1593 (1998).
- [5] Barman A., Ghosh M., Biswas S., De S.K. and Chatterjee S., "Charged ordered state and giant magnetoresistance in $\text{Pr}_{0.7}\text{R}_{0.1}\text{Ca}_{0.2}\text{MnO}_3$ (R=Y, Dy, Gd, Sm, Nd)." *J. Phys.: Condens. Matter* **10**, L199-L205, (1998).

Chapter 5

Conclusion and Suggestions for further work

5.1 Conclusion

- X-ray diffraction analyses show that all the investigated samples are homogeneous and of single crystalline structure.
- Samples show a metal-insulator transition with a peak in the electrical resistivity, at a temperature T_p .
- The above-mentioned metal- insulator transition temperature is generally very close to the Curie temperature, T_c , the ferromagnetic to paramagnetic transition. This sort of M-I transition can be explained within the framework of lattice distortion.
- The substitution of Ho in place of La and also the substitution of Ca in place of Ba for most of the investigated samples reduces metal –insulator transition temperature significantly.
- The presence of 0.7T magnetic field in this investigation increases M-I transition temperature only by few Kelvin. This means that the applied field is not sufficient for the suppression of spin fluctuations.
- In the present study, room temperature magnetoresistance is found to be low and is almost linear with field.
- Magnetoresistance measurements for the bulk samples show a sharp drop at low magnetic fields followed by a linear dependence at higher fields.
- The exhibited large MR effects in these compounds at low temperature and very low field might be associated with magnetic-domain based scattering or spin-polarized tunneling between adjacent grains.
- In $\rho(T)/\rho(RT) - T^{-1}$ plots for the present investigated samples suggest that conduction occurs through a thermally activated process.
- It was also observed that the activation energies increases slightly with the substitution of Ho & Ca in place of La & Ba and this is due to the lower size of Ho & Ca atom.

Chapter 5 Conclusion and Suggestions for Further Work

- In case of $\text{Ca} = 0.1$ for Ba in $\text{La}_{1-x}\text{Ho}_{0.2}\text{Ba}_{0.9}\text{Ca}_{0.1}\text{Mn}_2\text{O}_7$ sample the transition temperature is found to be very high and activation energy is found to be low compared to other compositions.

5.2 Suggestions for further work

Modern technologies are now governed by magnetic sensors, magnetoresistive read heads, magnetoresistive random access memory and magnetoresistive microphone etc. Here we have investigated the DC electrical and magnetic field dependent resistive properties of the layered manganites doped with the isovalent atoms on the La-site. All the samples show low-field magnetoresistive properties at low temperature. For the applications of these samples, more comprehensive experimental studies are needed. In our experimental work, all the samples were sintered in 1373 K (1100°C). With the variations of sintering temperature further study can be done to check their magnetoresistive properties. At present, it is well known that grain size, nuclear magnetic moments, magnetization, tolerance factors, susceptibility, polaron effects, spin waves, conduction electrons, phonons, and domain walls etc. are play the crucial rule in the manganites with which we will able to describe the transport properties such as temperature resistivity, low temperature dependent resistivity, optical conductivity, and thermal conductivity etc. and many other effects. Changes in the electronic structure induced by photons, electric fields or other means which are long lived (hysteric phase transitions) need to be explored and controlled especially in thin films for storage applications.

